



1 **Projected global tropospheric ozone impacts on vegetation under different**
2 **emission and climate scenarios**

3 Sicard Pierre¹, Anav Alessandro², De Marco Alessandra³, Paoletti Elena²
4

5 ¹ ACRI-HE, Sophia Antipolis, France

6 ² Institute of Sustainable Plant Protection, National Research Council, Sesto Fiorentino, Italy

7 ³ Italian National Agency for New Technologies, Energy and the Environment, C.R. Casaccia, Italy
8

9
10 **Abstract**

11 The impact of ground-level ozone (O₃) on vegetation is largely under-investigated at global
12 scale despite worldwide large areas are exposed to high surface O₃ levels and concentrations
13 are expected to increase in the next future. To explore future potential impacts of O₃ on
14 vegetation, we compared historical and projected O₃ concentrations simulated by six global
15 atmospheric chemistry transport models on the basis of three representative concentration
16 pathways emission scenarios (i.e. RCP 2.6, 4.5, 8.5). To assess changes in the potential O₃
17 threat to vegetation, we used the AOT40 metric. Results point out a significant overrun of
18 AOT40 in comparison with the recommendations of UNECE for the protection of vegetation.
19 In fact, many areas of the northern hemisphere show that AOT40-based critical levels will be
20 exceeded by a factor of at least 10 under RCP8.5. Changes in surface O₃ by 2100 range from
21 about + 4-5 ppb worldwide in RCP8.5 scenario to reductions of about 2-10 ppb in the RCP2.6
22 scenario. The risk of O₃ injury for vegetation decreased by 61% and 47% under RCP2.6 and
23 RCP4.5, respectively and increased by 70% under RCP8.5. Key biodiversity areas in South
24 and North Asia, central Africa and Northern America were identified as being at risk from
25 high O₃ concentrations. To better evaluate the regional exposure of ecosystems to O₃
26 pollution, we recommend the use of improved chemistry-climate modelling system, fully
27 coupled with dynamic vegetation models.

28
29 * Corresponding author: pierre.sicard@acri-he.fr

30
31 **Keywords:** AOT40, Ozone, Representative Concentration Pathways, O₃ injury on vegetation

32



33 Introduction

34 Tropospheric ozone (O₃) is a secondary air pollutant, i.e. it is not emitted as such in the air but
35 it is formed by reactions among precursors (e.g. CH₄, VOCs, NO_x). Ozone is an important
36 greenhouse gas resulting in a direct radiative forcing of 0.35-0.37 W m⁻² on climate (Shindell
37 et al., 2009; Ainsworth et al., 2012). Despite significant control efforts and legislation to
38 reduce O₃ precursor emissions, tropospheric O₃ pollution is still a major air quality issue over
39 large regions of the Globe (Lefohn et al., 2010; Langner et al., 2012; Young et al., 2013;
40 Cooper et al., 2014; EEA, 2015; Sicard et al., 2016a,b). Long-range transport of O₃ and its
41 precursors can elevate the local and regional O₃ background concentrations (Ellingsen et al.,
42 2008; Wilson et al., 2012; Paoletti et al., 2014; Derwent et al., 2015; Xing et al., 2015; Sicard
43 et al., 2016a). Therefore, remote areas such as the Arctic region, can be affected (Langner et
44 al., 2012). The current tropospheric O₃ levels (35-50 ppb in the northern hemisphere, NH) are
45 high enough to damage both forests and crops by reducing growth rates and productivity
46 (Paoletti et al., 2009; Wittig et al., 2009; Anav et al., 2011; Mills et al., 2011; Ashworth et al.,
47 2013; Proietti et al., 2016).

48

49 Increasing atmospheric CO₂, nitrogen deposition and temperatures enhance plant growth, and
50 increase primary production and greening of plants (Nemani et al., 2003; Zhu et al., 2016). At
51 the global scale, a widespread increase of greening and net primary production (NPP) is
52 observed over 25-50% of the vegetated area, while a decrease is observed over only 7% of the
53 Globe (Nemani et al., 2003; Zhu et al., 2016). In contrast, a previous modeling study over
54 Europe shows how O₃ reduces the mean annual gross primary production (GPP) by about
55 22% and the leaf area index by 15-20% (Anav et al., 2011). Similarly, Proietti et al (2016),
56 using different *in-situ* measurements collected over 37 European forest sites, found a GPP
57 decrease of 30% caused by O₃. At global scale, over the time period 1901-2100, GPP is
58 projected to decrease by 14-23% (Sitch et al., 2007). As a consequence of reduced
59 photosynthetic assimilation, the total biomass of trees is estimated to be decreased by 7%
60 under the current O₃ mean concentrations (40 ppb) and by 17% under the O₃ mean
61 concentrations expected in 2100 (97 ppb) compared to preindustrial O₃ levels (about 10 ppb,
62 Wittig et al., 2009). Wittig et al. (2009) also reported that the total tree biomass of
63 angiosperms was reduced by 23% at O₃ mean concentrations of 74 ppb, and by 7% at 92 ppb
64 for gymnosperms. High surface O₃ levels, exceeding 40 ppb, do occur in many regions of the
65 Globe with associated economic costs of several billion dollars per year (Wang and
66 Mauzerall, 2004; Ashmore, 2005). Ashworth et al. (2013) reported an annual loss of 3.5% for



67 wheat (very O₃-sensitive) and 1% for maize (more O₃-tolerant) for Europe in 2010 relative to
68 2000, while Holland et al. (2006) estimated a €4.5 billion loss in the production of 23
69 common crop species, due to surface O₃ exposure by 2020 relative to 2000.

70

71 The international Tropospheric Ozone Assessment Report (TOAR) establishes a state-of-the-
72 art and an up-to-date scientific assessment of global O₃ metrics for climate change, human
73 health and crop/ecosystem research (Lefohn et al. 2017). To assess the potential O₃ risk and
74 protect vegetation from O₃, different metrics are used: the European and US standard (AOT40
75 and W126, respectively) are based on exposure-based metrics, while flux-based metrics have
76 been introduced only recently (UNECE, 2010; Klingberg et al., 2014; EEA, 2015). Unlike the
77 exposure-based metrics, which only rely on the surface O₃ concentration, the flux-based
78 metrics were developed to quantify the accumulation of damaging O₃ taken up by vegetation
79 through the stomata over a species-specific phenological time-window. These metrics also
80 provide an information-rich tool in assessing the relative effectiveness of air pollution control
81 strategies in lowering surface O₃ levels worldwide (Monks et al., 2015). By reducing plant
82 photosynthesis and growth, high tropospheric O₃ levels will result in reduction in carbon
83 storage by vegetation and, *in fine* an indirect radiative forcing as a consequence of the CO₂
84 rising in the atmosphere (Sitch et al., 2007; Ainsworth et al., 2012). This CO₂ rising reduces
85 stomatal conductance which decreases O₃ flux into plants leading to increased O₃ levels in the
86 air of 3-4 ppb during the growing season over the NH by doubling of CO₂ concentration
87 (Fiscus et al., 2005; Sanderson et al., 2007).

88

89 Projected changes in tropospheric O₃ vary considerably among models (Stevenson et al.,
90 2006; Wild, 2007) and emission scenarios. In earlier studies, the emissions of O₃ precursors
91 were based on a high population growth, leading to very high projected surface O₃
92 concentrations by 2100 (Stevenson et al., 2000; Zeng and Pyle, 2003; Shindell et al., 2006).
93 The last emission scenarios, i.e. the Representative Concentration Pathways (RCPs) were
94 developed as part of the Fifth Assessment Report of the Intergovernmental Panel on Climate
95 Change (Meinshausen et al., 2011; van Vuuren et al., 2011; Cubasch et al., 2013; Myhre et
96 al., 2013). These scenarios include e.g. different assumptions on climate, energy access
97 policies, and land cover and land use changes (Arneth et al., 2008; Kawase et al., 2011;
98 Kirtman et al., 2013). Until now, studies on O₃ pollution impacts on terrestrial ecosystems are
99 either limited to a single model or to particular regions (e.g. Clifton et al., 2014; Rieder et al.,
100 2015) and only a few applications of global or regional models under the new RCPs scenarios



101 were carried out (Kelly et al., 2012). In the framework of the Atmospheric Chemistry and
102 Climate Model Intercomparison Project (ACCMIP), different simulations were performed by
103 Lamarque et al. (2013) and Young et al. (2013) from 16 global chemistry models.

104

105 A few issues about surface O₃, such as a better understanding of spatial changes and a better
106 assessment of O₃ impacts worldwide, are still challenging. To overcome these issues, the aim
107 of this study is to quantify, for the first time, the spatial and temporal changes in the projected
108 potential O₃ impacts on carbon assimilation of vegetation at global scale, by comparing the O₃
109 potential injury at present with that expected at the end of the 21st century from different
110 global chemistry models.

111

112 **Materials and Methods**

113

114 *ACCMIP models and RCP scenarios*

115

116 The global chemistry models used in this work have been developed under the ACCMIP
117 project. A detailed description of the selected models and of the emission scenarios (i.e.
118 RCPs) is included in Supplementary Information (SI). ACCMIP models have been widely
119 validated and used to evaluate projected changes in atmospheric chemistry and air quality
120 under different emission and climate assumptions (e.g. Lamarque et al., 2010; Fiore et al.,
121 2012; Bowman et al., 2013; Lee et al., 2013; Voulgarakis et al., 2013). Lamarque et al. (2013)
122 and Young et al. (2013) provided the main characteristics of 16 models and details for the
123 ACCMIP simulations. Although within the ACCMIP project 16 models are available, due to
124 the lack of hourly O₃ concentration here we only focus on 6 global chemistry models with
125 different configurations (Table 1).

126

127 The length of historical and RCP simulations vary between models, but for all models the
128 historical runs cover a period centered around 2000, while the time-slice of RCPs is centered
129 around 2100 (Table 1). As for each model we compare the mean change between the
130 historical and RCP simulations, a different length in the number of years used in the analysis
131 does not affect the results.

132

133 *Potential ozone injury on vegetation*

134

135 The O₃ exposure-based index, i.e. AOT40 (ppb h), is a metric used to assess the potential O₃
136 risk to vegetation from local to global scales (Emberson et al., 2014). It is computed as sum



137 of the hourly exceedances above 40 ppb, for daylight hours (8am-8pm) over species-specific
138 growing seasons (UNECE, 2010). A recent study over Europe showed how computing
139 AOT40 only over the growing season (i.e. April-September) would lead to an underestimation
140 of AOT40 up to 50% for conifer trees, while in case of deciduous trees the underestimation is
141 much smaller (< 5%, Anav et al., 2016). Besides, it should be noted that in Anav et al. (2016)
142 the AOT40 is computed year-round when the stomatal conductance is greater than 0. Here,
143 because of the lack of hourly meteorological data, we can only compute the AOT40 year-
144 round and during the daylight hours. In case of risk assessment, this approach would lead to a
145 relevant overestimation of AOT40, mainly over polluted area of NH. Nevertheless, since the
146 aim of this study is to compare how O₃ stress to vegetation changes between historical period
147 and future, the overestimation of AOT40 does not affect our results. Therefore, we computed
148 AOT40 as follows:

149

$$150 \text{ AOT40} = \int_{01\text{jan}}^{31\text{dec}} \max([O_3] - 40, 0) dt \quad (1)$$

151

152 where [O₃] is hourly O₃ concentration (ppb) simulated by the models at the lower model layer
153 and *dt* is time step (1h). The function "maximum" ensures that only values exceeding 40 ppb
154 are taken into account. The O₃ concentration to be used in AOT40 calculation should be at the
155 top of the canopy; however, most of models used here provide O₃ concentrations at 90-120 m.
156 Nevertheless, even if the O₃ concentration is simulated at different elevations above the sea
157 level, as for each model we compare the variation between present and future, the change is
158 consistent because the elevation is the same. For the protection of forests, a critical level of
159 5,000 ppb.h (or 5 ppm.h) is recommended by UNECE (2010). Within the 2008/50/CE
160 Directive, the critical level for agricultural crops (3 ppm.h) is adopted as the long-term
161 objective value for the protection of vegetation by 2020.

162

163 From the AOT40, a factor of risk for forests and crops can be computed (Anav et al. 2011;
164 Proietti et al. 2016). Thus, the potential O₃ impact on photosynthetic assimilation (IO₃) is
165 expressed as following:

166

$$167 \text{ IO}_3 = \alpha \times \text{AOT40} \quad (2)$$

168

169 where α is an empirically derived O₃ response coefficient representing the proportional
170 change in photosynthesis per unit of ozone-uptake (Anav et al., 2011). The coefficient for
171 coniferous trees ($0.7 \times 10^{-6} \text{ mm}^{-1} \text{ ppb}^{-1}$) and crops ($3.9 \times 10^{-6} \text{ mm}^{-1} \text{ ppb}^{-1}$) are based on the



172 regressions of the ozone-uptake response curves (Reich, 1987), while the coefficient for
173 deciduous trees and other vegetation types ($2.6 \times 10^{-6} \text{ mm}^{-1} \text{ ppb}^{-1}$) is based on Ollinger et al.
174 (1997). From changes in the risk factor, we can highlight potential risk areas for vegetation.

175

176 **Results and Discussion**

177 Although differences in the simulated global O_3 spatial pattern were previously discussed and
178 analyzed (e.g. Lamarque et al., 2013), we show the mean annual O_3 concentration at the lower
179 model layer in Figure 1 because O_3 concentration explains AOT40 patterns. Then, in Figure 2
180 we show and discuss the AOT40 spatial and temporal distribution from the ACCMIP models
181 for the historical and RCPs simulations, and finally in Figure 3 we show the percentage of
182 variation of IO3, i.e. the change in the potential impact of O_3 on vegetation for the ACCMIP
183 models computed comparing the RCPs simulations with historical runs. A detailed description
184 of each figure, model by model, is included in Supplementary Information (SI).

185

186 **Spatial pattern of historical ozone concentration and AOT40**

187 The highest surface O_3 concentrations (Fig. 1) and potential O_3 injury (Fig. 2) are found in the
188 NH, highlighting a hemispheric asymmetry. The multi-models O_3 mean concentration,
189 averaged over the land points of the domain, is 37.9 ± 4.3 ppb in NH and 22.9 ± 3.8 ppb in
190 SH (Table 3a). The NH extratropics (i.e. mid-latitudes beyond the tropics) has 65% more O_3
191 than the SH extratropics (data not shown). The highest AOT40 values are found in the NH,
192 with an averaged AOT40 of 24.8 ± 10.1 ppm.h in NH and 2.5 ± 1.7 ppm.h in SH (Table 3a).

193

194 According to previous studies, the annual mean background O_3 concentrations at NH mid-
195 latitudes range between 35 and 50 ppb during the end of the 20th century (e.g. Cooper et al.,
196 2012; IPCC, 2014; Lefohn et al. 2014). Similarly, we found historical surface O_3 mean
197 concentrations ranging between 35 and 50 ppb and 35-50 ppm.h for AOT40 in the NH, with
198 the highest values occurring over Greenland and in the latitude band 15-45°N, particularly
199 around the Mediterranean basin, Near East, Northern America and over the Tibetan plateau (>
200 50 ppb and 70 ppm.h) while the lowest O_3 burden (15-30 ppb, < 20 ppm.h) was recorded in
201 SH, particularly over Amazon, African and Indonesian rainforests. Tropospheric O_3 has a
202 significant source from stratospheric O_3 (Parrish et al., 2012) and it can be transported by the
203 large-scale Brewer-Dobson overturning circulation, i.e. an upward motion from the tropics
204 and downward at higher latitudes, resulting in higher O_3 concentrations in the extratropics



205 (Hudson et al., 2006; Seidel et al., 2008; Parrish et al., 2012). The six models are able to
206 reproduce the spatial pattern of O₃ concentration and thus AOT40 worldwide.

207

208 The highest historical O₃ mean concentrations are observed in GFDL-AM3 and the lowest are
209 found in MIROC-CHEM. In the early 2000s, the maximum global O₃ mean concentration (39
210 ppb) in GFDL-AM3 is associated to the lowest annual total NO_x emissions (46.2 Tg, Table
211 2a) and low LNO_x (4.4 Tg) while the minimum global O₃ mean concentration (28 ppb) in
212 MIROC-CHEM is related to the highest emissions of total NO_x per year (57.3 Tg) and
213 erroneously high LNO_x (9.7 Tg per year, Lamarque et al., 2013). MIROC-CHEM simulates
214 58 gaseous species in the chemical scheme with constant present-day biogenic VOCs
215 emissions while GFDL-AM3 simulates 81 species (Stevenson et al., 2012; Lamarque et al.,
216 2013). In GISS-E2-R, the hemispheric asymmetry in O₃ is more important with e.g. a mean
217 concentration of 22 ppb in SH and 42 ppb in NH. A stronger global AOT40 mean (26 ppm.h)
218 is observed in GISS-E2-R and the lowest (7 ppm.h) in MIROC-CHEM for historical
219 simulations. Model-to-model differences are observed due to different natural emissions of O₃
220 precursors (e.g. lightning NO_x) and the used chemical schemes.

221

222 Higher O₃ burdens (mean concentration > 50 ppb, AOT40 >70 ppm.h) are simulated at high-
223 elevation areas, e.g. at Rocky and Appalachian Mountains and over the Tibetan plateau (Fig.
224 1, Fig. 2). At high-elevation, solar radiation, biogenic VOC emission, exchange between free
225 troposphere and boundary layer, and stratospheric O₃ intrusion within the troposphere are
226 more important than at the surface layer (Steinbacher et al. 2004; Kulkarni et al., 2011; Lefohn
227 et al., 2012). Altitude reduces the O₃ destruction by deposition and NO (Chevalier et al.,
228 2007). In addition, due to the high elevation, ambient air remains colder and dryer in summer,
229 leading to lower summertime O₃ losses from photolysis (Helmig et al., 2007). The high-
230 elevation areas, characterized by higher O₃ burdens, are well simulated in GISS-E2-R and
231 MOCAGE models.

232

233 The Tibetan plateau, so-called “ozone valley”, is the highest plateau in the world, with a mean
234 height of 4000 m a.s.l. (Tian et al., 2008) with strong thermal and dynamic influences on
235 regional and global climate (Chen et al. 2011). High surface O₃ mean concentrations (40-60
236 ppb) were reported in previous studies (e.g. Zhang et al., 2004; Bian et al., 2011; Guo et al.,
237 2015; Wang et al., 2015). Although this region is remote, road traffic, biofuel energy source,
238 coalmines and trash burning are prevalent. These pollution sources contribute to significant



239 amount of NO_x, CO and VOCs (Wang et al., 2015). The high O₃ levels are attributed to the
240 combined effects of high-elevation surface, thermal and dynamical forcing of the Tibetan
241 plateau and *in-situ* photochemical production in the air trapped in the plateau by surrounding
242 mountains (Guo et al., 2015; Wang et al., 2015). The dynamic effect, associated with the
243 large-scale circulation, is more important than the chemical effect (Tian et al., 2008; Liu et al.,
244 2010) and responsible for the high O₃ levels over the Tibetan plateau. The six models are able
245 to well reproduce the high surface O₃ mean concentrations (> 50 ppb) over the Tibetan
246 plateau.

247

248 Higher O₃ mean concentrations (> 60 ppb) are also observed in Southwestern U.S., at the
249 stations inland close to Los Angeles, in Northeastern U.S. and East Asia (e.g. Beijing) (Fig.
250 1). The American Southwest is an O₃ precursor hotspot where the industrial sources emit CH₄
251 and VOCs into the air (Jeričević et al., 2013) and the eastern and northern desert areas have
252 higher ambient O₃ than urban areas of southern California due to four factors: on-shore winds,
253 gasoline reformulation, eastward population expansion and nighttime air chemistry (Arbaugh
254 and Bytnerowicz, 2003). The surface concentrations show higher O₃ levels in areas downwind
255 of O₃ precursor sources, i.e. urban and well-industrialized areas, at distances of hundreds or
256 even thousands of kilometers due to transport of O₃ and precursors, including “reservoir”
257 species such as PAN, lower O₃ titration by NO and higher biogenic VOC emission (Wilson et
258 al., 2012; Paoletti et al., 2014; Monks et al., 2015; Sicard et al., 2016a). The higher O₃ levels
259 in areas downwind of O₃ precursor sources are well simulated in GISS-E2-R and MOCAGE
260 models.

261

262 In the lower troposphere, O₃ can be removed by a large number of chemical reactions and by
263 dry deposition (Sicard et al., 2016c). The O₃ dry deposition rates range from 0.01-0.05 cm s⁻¹
264 (oceans and snow) to 0.15-1.80 cm s⁻¹ for mixed wood forests (Wesely and Hicks, 2000;
265 Zhang et al., 2003). The model performance is also related to the parameterization of the dry
266 deposition rates.

267

268 Over Greenland, mean O₃ concentrations during the historical runs, ranged from 40 to 55 ppb
269 (Fig. 1) except in MIROC-CHEM (20-25 ppb). Similarly, Helmig et al. (2007) reported
270 annual mean of surface O₃ concentrations of 47 ppb over Greenland between 2000 and 2005,
271 particularly at the high-elevation Summit station (3200 m a.s.l.). Several investigations, about
272 snow photochemical and oxidation processes over Greenland, concluded that photochemical



273 O₃ production can be attributed to high levels of reactive compounds (e.g. oxidized nitrogen
274 species) present in the surface layer during the sunlit periods due to local sources e.g. NO_x
275 enhancement from snowpack emissions, Peroxyacetyl nitrate (PAN) decomposition, boreal
276 forest fires or ship emissions (Granier et al., 2006; Stohl et al., 2007; Legrand et al., 2009;
277 Walker et al., 2012). PAN to NO_x ratio increases with increasing altitude and latitude (Singh
278 et al., 1992). The PAN reservoir for NO_x may be responsible for the increase in surface
279 O₃ concentrations at high latitudes (Singh et al., 1992). Local O₃ production does not appear to
280 have an important contribution to the ambient high O₃ levels (Helmig et al., 2007), however
281 the long-range O₃ transport can elevate the background concentrations measured at remote
282 sites, e.g. Greenland (Ellingsen et al., 2008; Derwent et al., 2010). Low dry deposition rates
283 for O₃, the downward transport of stratospheric O₃, the photochemical local production and
284 the large-scale transport (Legrand et al., 2009; Walker et al., 2012; Hess and Zbinden, 2013)
285 are known factors to explain higher O₃ pollution over Greenland.

286

287 The surface O₃ concentrations (> 40 ppb) and AOT40 (> 60 ppm.h) are higher over deserts,
288 downwind of O₃ precursor sources (e.g. Near East, Sierra Nevada, Colorado Desert), due to
289 lower O₃ dry deposition fluxes, O₃ precursors long-range transport from urbanized areas and
290 high insolation. Around the Mediterranean basin, elevated AOT40 values (> 60 ppm.h) are
291 recorded, mainly due to the industrial development, road traffic increment, high insolation,
292 sea/land breeze recirculation and O₃ transport (Sicard et al., 2013). All models, except
293 MIROC-CHEM, are able to well reproduce the high surface O₃ mean concentrations over
294 Greenland and over deserts.

295

296 **Projected changes in ozone concentration and AOT40**

297

298 Recent studies display a mean global increase in background O₃ concentration from a current
299 level of 35-50 ppb (e.g. IPCC, 2014; Lefohn et al. 2014) to 55-65 ppb (e.g. Wittig et al., 2007)
300 and up to 85 ppb at NH mid-latitudes by 2100 (IPCC, 2014). During the latter half of the 20th
301 century surface O₃ concentrations have increased markedly at NH mid-latitudes (e.g. Oltmans
302 et al., 2006; Parrish et al., 2012; Paoletti et al., 2014), mainly related to increasing
303 anthropogenic precursor emissions related to economic growth of industrialized countries
304 (e.g. Lamarque et al., 2005). Our results indicate that the future projections of the mean
305 tropospheric O₃ concentrations and AOT40 vary considerably with the different scenarios and
306 models (Fig. 1 and 2). The six models simulate a decrease of O₃ concentration by 2100 under
307 the RCP2.6 and RCP4.5 scenarios, and an increase under the RCP8.5 scenario (Lamarque et



308 al., 2011). In our study, the averaged relative changes in surface O₃ concentration means (and
309 AOT40) for the different RCPs are: -21% (-75%) for RCP2.6, - 10% (-50%) for RCP4.5 and
310 + 14% (+69%) for RCP8.5 with a strong disparity between both hemispheres, e.g. - 8% in SH
311 and - 25% in NH for RCP2.6 (Tables 3b-c). RCP8.5 is the only scenario to show an increase
312 in global background O₃ levels by 2100 (+ 23% in SH and + 11% in NH).

313
314 Under the RCP2.6 scenario, all models predict that tropospheric O₃ will strongly decrease
315 worldwide, except in Equatorial Africa where higher O₃ levels are observed in GFDL-AM3,
316 GISS-E2-R and MOCAGE. In CESM-CAM, GFDL-AM3 and MIROC-CHEM, a
317 homogeneous decrease in O₃ burden is simulated worldwide while in GISS-E2-R, MOCAGE
318 and UM-CAM, the strongest decrease in surface O₃ mean concentrations are found where
319 high historical O₃ concentrations were reported. Under RCP4.5 scenario, the surface O₃ mean
320 concentrations and AOT40 values are lower than historical runs worldwide for all models
321 except in MOCAGE where deterioration is observed over Canada, Greenland and East Asia.
322 For all models, the surface O₃ levels and AOT40 are higher for RCP8.5 as compared to
323 historical runs and the highest increases occur in the Northwestern America, Greenland,
324 Mediterranean basin, Near East and East Asia. The AOT40 values, exceeding 70 ppm.h, are
325 found over the Tibetan plateau and in Near East and over Greenland. For RCP8.5, GFDL-
326 AM3 is the most pessimistic model and MIROC-CHEM the most optimistic. By the end of
327 the 21st century, similar patterns are evident for RCP4.5 compared to RCP2.6 and RCP4.5
328 simulation is intermediate between RCP2.6 and RCP8.5 ones.

329
330 For all models and RCPs, the O₃ hot-spots (mean concentrations > 50 ppb and AOT40 > 70
331 ppm.h) are over Greenland and South Asia, in particular over the Tibetan plateau. The highest
332 increases are observed in NH, in particular in Northwestern America, Greenland, Near East
333 and South Asia (> 65 ppb). For the three RCPs, no significant change in tropospheric O₃ is
334 observed in SH and the SH extratropics makes a small contribution to the overall change.

335
336 A recent global study showed the geographical patterns of surface air temperature differences
337 for late 21st century relative to the historical run (1986-2005) in all RCP scenarios (Nazarenko
338 et al., 2015). The global warming in the RCP2.6 scenario is 2-3 times smaller than RCP4.5
339 scenario and 4-5 times smaller than RCP8.5 scenario (Nazarenko et al., 2015). For the three
340 RCPs, the greatest change is observed over the Arctic, above latitude 60°N, and in the latitude
341 band 15-45°N (IPCC, 2014; Nazarenko et al., 2015). The least warming is simulated over the



342 large area of the Southern Ocean. For RCP8.5 scenario, the global pattern of surface O₃ levels
343 and AOT40 (Fig. 1-2) is similar to surface air temperature increase distribution. For RCP8.5,
344 significant increases in air temperature are simulated over latitude 60°N and over the Tibetan
345 plateau (more than 5°C). An increase of 4-5°C over the Near East, East and South Asia, North
346 and South Africa and Canada are simulated as well as + 1-3°C for the rest of the world
347 (Nazarenko et al., 2015). The tropospheric warming is stronger in the latitude band 15-45°N
348 (Seidel et al., 2008) and Hudson et al. (2006) have demonstrated that O₃ trends over a 24-year
349 period in the NH are due to trends in the relative area of the tropics and mid-latitudes and
350 Polar Regions. All models are able to reproduce the global pattern of air temperature changes
351 distribution in agreement with surface O₃ concentrations changes.

352

353 The spread in precursor emissions (e.g. VOCs, NO_x, CO) is due to the range of representation
354 of biogenic emissions (NO_x from soils and lightning, CO from oceans and vegetation) as well
355 as the complexity of chemical schemes in particular for NMVOCs simulations (e.g. isoprene)
356 from explicitly specified to fully interactive with climate. RCP2.6 scenario has the lowest O₃
357 precursor concentrations, and RCP8.5 has relatively low NO_x, CO and VOCs emissions, but
358 very high CH₄ (Table 2b). The global emissions of NO_x (-44%), VOCs (-5%) CO (-40%) and
359 CH₄ burden (-27%) decline, while LNO_x increase by e.g. 7% under RCP2.6 (Table 2b). The
360 CO (-32%) and NO_x (-20%) emissions have decreased while LNO_x (+33%), VOCS (+1%)
361 and CH₄ burden have increased (+120%) under RCP8.5 scenario (Table 2b). The GISS-E2-R
362 model shows a greater degree of variation than other models, with a stronger increase in CH₄
363 burden (+ 153%) and in VOCs emissions (+ 20%) for RCP8.5 (Table 2b).

364

365 Excluding CH₄ burden and VOCs emissions, all the RCPs include reductions and
366 redistributions of O₃ precursor emissions throughout the 21st century, due to the air pollution
367 control strategies worldwide. The changes in CH₄ burden are due to the different climate
368 policies in model assumptions. In RCP2.6, CH₄ emissions decrease steadily throughout the
369 century, in RCP4.5 it remain steady until 2050 and then decrease (Voulgarakis et al., 2013)
370 and in RCP8.5 (no climate policy) it rapidly increase compared to 2000. Methane burdens are
371 fixed in the models with no sources, except for the GISS-E2-R simulations in which surface
372 CH₄ emissions are prescribed for future rather than concentrations (Shindell et al., 2012). The
373 model chemical schemes vary greatly in their complexity, mainly due to the NMVOCs
374 simulations (Young et al. 2013). Isoprene dominates the total NMVOCs emissions (Guenther
375 et al., 1995). Inversely to other models with constant present-day isoprene emissions, the



376 GISS-ES2-R simulations incorporate climate-driven isoprene emissions, with greater BVOC
377 emissions by 2100 and a positive change in total VOCs emissions across RCPs, related to the
378 positive correlation between air temperature and isoprene emission (e.g. Guenther et al., 2006;
379 Arneth et al., 2011; Young et al., 2013).

380

381 For RCP2.6 and RCP4.5 scenarios, there is a widespread decrease in O₃ in NH by 2100. The
382 overall decrease in O₃ concentration and AOT40 means for RCP4.5 are about half of that
383 between RCP2.6 and the historical simulation. For both scenarios, the changes are dominated
384 by the decrease in O₃ precursor emissions in the NH extratropics compared to historical
385 simulations (Table 2b). In NO_x saturated areas, annual mean O₃ will slightly increase as a
386 result of a less efficient titration by NO, but the overall O₃ burden will decrease substantially
387 at hemispheric scale over time (Gao et al., 2013; Querol et al., 2014; Sicard et al., 2016a). In
388 RCP4.5, Gao et al. (2013) showed that the largest decrease in O₃ (4-10 ppb) occurs in summer
389 at mid-latitudes in the lower troposphere while the O₃ concentrations undergo an increase in
390 winter. During the warm period, the photochemistry plays a major role in the O₃ production,
391 suggesting that the reduction in surface O₃ concentrations is in agreement with the large
392 reduction in anthropogenic O₃ precursor emissions (Sicard et al., 2016a) reducing the extent
393 of regional photochemical O₃ formation (e.g. Derwent et al., 2013; Simpson et al., 2014).
394 Titration effect was also reported by Collette et al. (2012) over Europe by using six chemistry
395 transport models.

396

397 The O₃ increase can be also driven by the net impacts of climate change, i.e. increase in
398 stratospheric O₃ intrusion, changing LNO_x and impacting reaction rates, through sea surface
399 temperatures and relative humidity changes (Lau et al., 2006; Voulgarakis et al., 2013; Young
400 et al., 2013).

401

402 Under the RCP8.5 scenario, the increase in surface O₃ concentrations, by 14% on average, can
403 be attributed to the higher CH₄ emissions coupled with a strong global warming, exceeding
404 2°C, and a weakened NO titration by reducing NO_x emissions (Stevenson et al., 2013; Young
405 et al., 2013). The global CH₄ burden are 27% and 5% lower than 2000, for the RCP2.6 and
406 RCP4.5 scenarios respectively while for RCP8.5, the total CH₄ burden has more than doubled
407 compared to early 2000s and LNO_x emissions increased by 33% (Table 2b). In addition,
408 stronger increases are found over the high-elevation Himalayan Plateau reflecting increased
409 exchange with the free troposphere or stratosphere (Lefohn et al., 2012; Schnell et al., 2016).



410 Several studies reported an increase in the stratospheric O₃ influx and higher stratospheric O₃
411 levels in response to a warming climate (e.g. Hegglin and Shepherd, 2009; Zeng et al., 2010).
412 The downwards O₃ transport from the stratosphere is an important source of tropospheric O₃
413 (Hsu and Prather, 2009; Tang et al., 2011), therefore, stratospheric O₃ recovery also plays a
414 partial role (e.g. + 11% for RCP8.5) in surface O₃ burden pattern. As an example, in
415 MOCAGE, smaller reduction in global O₃ mean concentrations (-13%) and higher increase in
416 stratospheric O₃ inputs (+20%) are observed for RCP2.6 (Table 3b). Similarly, for RCP8.5,
417 the highest increase in O₃ mean concentrations (+23%) and stratospheric O₃ (+24%) are
418 recorded in MOCAGE. In addition, lightning NO_x emissions show significant upward trend
419 from 2000 to 2100, in particular for the strongest warming scenario (RCP8.5) with greater
420 convective and lightning activity (e.g. Williams, 2009; Lamarque et al., 2013). For RCP8.5, a
421 reduction in surface O₃ concentrations is also simulated over the equatorial region, where the
422 increased relative humidity, in a warmer climate, increases the O₃ loss rate (e.g. Johnson et
423 al., 1999; Zeng and Pyle, 2003).

424

425 **Risk areas for vegetation under RCP scenarios**

426

427 Figure 3 shows the changes in the potential O₃ injury between present and future. It should be
428 noted that a zero percentage of change (i.e. no change) for IO₃, is simulated in sparsely
429 vegetated regions (e.g. Gobi, Sahara, Near East, Western plateau and Greenland), while the
430 change can be higher than 100% when the historical O₃ concentrations are lower than 40 ppb
431 (i.e. AOT₄₀ = 0 and IO₃ = 0) and the O₃ concentrations exceed 40 ppb under RCPs (i.e.
432 AOT₄₀ > 0, IO₃ > 0).

433

434 The potential O₃ impact for vegetation strongly decreases in NH for RCP2.6, except in
435 MOCAGE where a slight increase in the risk factor (+ 15 %) is simulated at high latitudes and
436 in South Asia. Conversely, the areas where the risk for vegetation increases (> 60 %) occur
437 over Africa (+ 15% to + 60%) for all models, except in CESM-CAM where no change is
438 observed across Africa. Under RCP4.5 scenario, the strongest increase in potential risk for
439 vegetation (> + 60 %) is simulated by MOCAGE, markedly different from the other models,
440 above the latitude 50°N. For all models, the potential O₃ impact for vegetation increases
441 across Africa, from - 15% to + 60% while slight decreases or no change occur worldwide.
442 Under RCP8.5 scenario, an increase of average O₃ over a significant part of the domain is
443 simulated, therefore the exposure to O₃ pollution and impacts on vegetation will increase
444 worldwide by 2100. An increase of the O₃ impacts on vegetation is simulated in Northern



445 U.S., South America, Asia and Africa while a reduction in particular over Eastern U.S. and
446 Southeastern China, and a slight increase (+ 15%) or decrease (- 15%) over Europe depending
447 on the model, are simulated.

448 In summary, compared to the historical simulations, the averaged relative changes in the O₃
449 risk factor for the different RCPs are: - 61% for RCP2.6, - 47% for RCP4.5 and + 70% for
450 RCP8.5 (Table 3d). We thus find a significant reduction in risk for vegetation for both
451 RCP2.6 and RCP4.5 scenarios, except in South Africa and at high-latitudes in MOCAGE
452 simulations, and a strong increase in global risk under RCP8.5. Under RCP2.6 and RCP4.5
453 scenarios, IO₃ slightly increases in Africa and over North America and Asia (> latitude 60°N)
454 in MOCAGE. The risk increases over the few areas where the O₃ concentrations increased
455 between the historical period and 2100. Under both scenarios, the strongest reductions in risk
456 are observed over Amazon, Central Africa and South Asia, i.e. where the O₃ concentrations
457 have strongly declined between historical period and 2100. Under the RCP8.5, the areas
458 where the highest projected O₃ mean concentrations are simulated (e.g. Greenland, deserts)
459 are not associated to an increase in IO₃ due to the absence of vegetation. Under RCP8.5, IO₃
460 increases worldwide while a reduction is simulated over Southeast North America, northern
461 Amazon, Central Africa and Southeast Asia, and a slighter reduction or a slight increase is
462 simulated over Western Europe (depending on the model).

463

464 The spatial pattern of IO₃ is consistent with previous analyses on climate change and O₃
465 impacts on vegetation (e.g. Nemani et al., 2003; Zhu et al., 2016), i.e. the highest reduction in
466 risk for vegetation, in particular under RCP8.5, occurs over areas where a strong increase in
467 greening, LAI and NPP is observed due to global change and where a reduction in O₃ mean
468 concentrations is found by 2100 (Fig. 1). The regions with the largest greening trends are in
469 Southeast North America, northern Amazon, Europe, Central Africa and Southeast Asia with
470 an average increase of the observed LAI exceeding 0.25 m² m⁻² per year (Zhu et al., 2016).
471 The CO₂ fertilization effects (70%), nitrogen deposition (9%) and climate change (8%)
472 explain the observed greening trend (Zhu et al., 2016). The changing climate alone produces
473 persistent NPP increases and the regions with the highest increase in NPP, ranging from 1.0-
474 1.5% per year, are in Southeast North America, northern Amazon, Western Europe, Central
475 Africa and South Asia (Nemani et al., 2003). NPP increased by 6% globally between 1982
476 and 1999 and the highest increases are observed in tropical regions, with more than 1.5% per
477 year over Amazon rainforest which accounts for 42% of the global NPP increase (Nemani et



478 al., 2003). Amazon rainforest is one region where the effects are statistically significant. This
479 is particularly important owing to the role of the Amazon rainforests in the global carbon
480 cycle (Zhu et al., 2016). In these areas, the increasing effect of a warming climate on forests
481 (e.g. increase of greening, LAI) is higher than the reduction in GPP due to O₃. Inversely, the
482 risk for vegetation increases in particular in Africa, e.g. western Africa along the Gulf of
483 Guinea, in South Brazil and over high-latitudes regions (> 60°N) in North America and Asia
484 where a reduction or a slight increase in LAI (from - 0.05 to + 0.03 m² m⁻² per year) and
485 strong decreases, by 1.0-1.5% per year, in NPP are simulated (Nemani et al., 2003; Zhu et al.,
486 2016).

487

488 Our results are not in agreement with the high GPP reduction, due to O₃ effects, simulated by
489 Sitch et al. (2007) between 1901 and 2100, with a projected GPP reduction exceeding 30%
490 over Western Europe, eastern and western North America, Amazon, central Africa and East
491 Asia where higher surface O₃ mean concentrations were projected. Previous studies reported
492 that the reductions in GPP simulated by Sitch et al. (2007) are overestimated up to six times
493 (Ren et al., 2011; Zak et al., 2011; Kvaleveg and Myhre 2013), mainly due to the lack of
494 empirical data about the response of different species to O₃, the fact that a few experiments
495 have shown no response, e.g. grasslands (Bassin et al., 2013), and the non-inclusion of the
496 nitrogen limitation of growth (Kvaleveg and Myhre, 2013).

497

498 The projected land covers widely vary under RCPs (Betts et al., 2015). In RCP2.6 scenario,
499 the ground surface covered by croplands increases as a result of bio-energy production, with a
500 more-or-less constant use of grassland. The RCP4.5 scenario focuses on global reforestation
501 programs as part of global climate policy, as a result, the use of cropland and grassland
502 decreases. Under RCP8.5, an increase in croplands and grasslands is applied mostly driven by
503 an increasing global population (van Vuuren et al., 2011). Generally, the risk for vegetation
504 strongly increases over shrublands (e.g. high-latitude region, Australia, South Africa) and
505 savannas (e.g. South Brazil, Africa) and the risk decreases over forests, strongly over
506 evergreen broadleaf forest and deciduous woodland over Africa and Amazon rainforests, and
507 slighter over needleleaf forests in Northern America (Canada) and Northern Asia. The risk
508 slightly decreases or slightly increases over grasslands (Central Asia and central Africa and
509 U.S.). The largest decreases (50-80%) under RCP8.5 occur in Eastern U.S., Europe and
510 Southeastern China, where the ground is mainly dominated by croplands, in all models except
511 CESM-CAM.



512 **Conclusions**

513 From six global atmospheric chemistry transport models, we illustrate the changes, i.e.
514 differences for late 21st century relative to the historical run, in ground-level O₃
515 concentrations and vegetation impact metric (AOT40). *In fine*, the potential O₃ impacts on
516 vegetation worldwide are investigated to define potential risk areas for vegetation at global
517 scale by 2100.

518

519 The six models are able to well reproduce the spatial pattern of historical O₃ concentration
520 and AOT40 at global scale, in particular GISS-E2-R and MOCAGE are able to simulate the
521 higher O₃ levels in areas downwind of precursor sources and at the high-elevation areas. The
522 model outputs emphasize the strong asymmetry in the tropospheric O₃ distribution between
523 NH and SH; substantially higher O₃ mean concentrations are observed in the NH (ca. 38 ppb),
524 particularly in the latitude band 15-45°N, than in the SH (ca. 23 ppb). The natural emissions
525 of O₃ precursors (e.g. lightning NO_x, CO from oceans, isoprene) as well as the complexity of
526 chemical schemes are significant sources of model-to-model differences.

527

528 In this study, the projected mean tropospheric O₃ concentrations and AOT40 dependent on
529 global and regional emission pathways. Compared to early 2000s, the results suggest changes
530 in surface O₃ of -9.5 ± 2.0 ppb (NH) and -1.8 ± 2.1 ppb (SH) in the cleaner RCP2.6 scenario
531 and of $+4.4 \pm 2.8$ ppb (NH) and $+5.1 \pm 2.1$ ppb (SH) in RCP8.5 scenario. For RCP2.6 and
532 RCP4.5, absolute decreases are observed for the Mediterranean basin and the Western U.S.
533 due to less precursor emissions in the NH extratropics (e.g. reduction of 5-7 ppb over
534 Europe). Smaller reduction in surface O₃ levels in South and East Asia highlight the smaller
535 changes in O₃ precursor emissions due to the recent emission growth in this region (e.g.
536 Zhang et al., 2009; Xing et al., 2015). For RCP8.5, all models show climate-driven increases
537 in ground-level O₃ in particular over the Western U.S, Greenland, South Asia and Northeast
538 China. The changes in surface O₃ over North America and Europe ranged from + 1-5 ppb
539 under RCP8.5. South Asia sees the greatest increase, up to more than 10 ppb for RCP 8.5. The
540 O₃ increase can be attributed to substantial increase in CH₄ emissions coupled with a strong
541 global warming, exceeding 2°C, and a weakened NO titration and a greater stratospheric O₃
542 influx (Kawase et al., 2011; Wild et al., 2012; Young et al., 2013). A decline in CH₄
543 emissions will undoubtedly benefit future O₃ control.

544



545 The current surface O₃ levels (35-50 ppb in NH) are high enough to damage both forests and
546 crops. About 50% of forests, grasslands and croplands might be exposed to high O₃ levels by
547 the end of the 21st century (Sitch et al., 2007; Wittig et al. 2009). Most important results from
548 the study are the significant overrun of exposure metric (AOT40) in comparison with the
549 AOT40-based critical level for the protection of forests (5 ppm.h) and crops (3 ppm.h). The
550 global models suggest that exposure-based critical levels will be exceeded over many areas of
551 the NH, and in parts of North America, East and South Asia they may be exceeded by a factor
552 exceeding 10 under RCP8.5. The critical level were defined for boreal and temperate
553 deciduous tree species, i.e. more consistent for regions in the latitude band 35-60°N. To
554 protect vegetation, the current AOT40 index appears inadequate for a realistic quantification
555 of O₃ impacts on vegetation (Paoletti and Manning, 2007; Mills et al., 2011; De Marco et al.,
556 2015; Sicard et al., 2016b,c). As a result, in the last decade, the United Nations Convention on
557 Long-Range Transboundary Air Pollution (CLRTAP) has introduced the flux-based metric
558 for vegetation protection against effects of O₃, taking into account the modifying effects of
559 multiple climatic and phenological factors on O₃ uptake (Paoletti and Manning, 2007; Sicard
560 et al., 2016b,c).

561 Ozone may be a major threat to biodiversity over large regions of the world (Sicard et al.,
562 2016b), however the size of these areas remains uncertain. The potential O₃ impact on
563 assimilation, IO₃, provides a clear indicator of the potential risk to vegetation. The risk for
564 vegetation decreases by about 61% and 47% under RCP2.6 and RCP4.5, respectively and
565 increases by 70% under RCP8.5, compared to early 2000s over the whole domain by 2100
566 and that the potential risk areas for vegetation vary worldwide according to the dominant
567 vegetation cover. The strongest increase of the O₃ impacts on vegetation is simulated in
568 Northern America and Asia and central Africa. The highest reduction in risk for vegetation
569 (i.e. Southeast North America, the northern Amazon, Central Africa and Southeast Asia)
570 occurs over areas where a strong increase in greening, LAI and NPP is observed and where a
571 reduction in O₃ mean concentrations is found by 2100.

572

573 Trees possess a defence capacity, e.g. through antioxidant activity and a capacity of repairing
574 injured tissues (Paoletti, 2007). The short-term response to O₃ is a reduction in productivity of
575 crops and forests and long-term changes in community composition could be observed due to
576 species-specific O₃-sensitivity (Wittig et al., 2009). Generally, deciduous woodland are highly
577 O₃-sensitive risk areas, grasslands and needleleaf forests are moderately O₃-sensitive risk



578 areas while the lower risk areas include evergreen broadleaf forests . However, crops are more
579 sensitive to O₃ exposure than trees and deciduous trees are more sensitive than coniferous
580 trees with lower stomatal conductance (Felzer et al., 2004; Ren et al., 2007; Wittig et al. 2009;
581 Anav et al., 2011). To efficiently protect vegetation against O₃ pollution, suitable standards
582 taking into account the detoxification processes (e.g. flux-based metric) are urgently needed.

583

584 As the vegetation atmosphere feedbacks are still under investigated, e.g. impacts of changes
585 of vegetation on air chemistry, we recommend the use of improved chemistry-climate
586 modelling system, fully coupled with dynamic vegetation models, to perform high resolution
587 simulations and to better evaluate the regional exposure of ecosystems to air pollution.

588

589 The risk reduction is possible through climate-change mitigation, e.g. reductions in air
590 pollution, and adaptation actions. An efficient reduction in overall O₃ levels is expected over
591 North America and Europe in all RCP scenarios and worldwide if CH₄ emissions are reduced
592 (e.g. Kirtman et al., 2013; Pfister et al., 2014; Schnell et al., 2016). However, the increasing
593 effect of a warming climate on surface O₃ concentrations is higher than the reduction
594 achieved by the decline in O₃ precursor emissions (Revell et al., 2015; Hendriks et al., 2016),
595 therefore, climate change and the measures and policies in e.g. Asia will need to be factored
596 into future O₃ policies (Wilson et al., 2012; Lefohn and Cooper, 2015). Many ecosystems
597 worldwide are unprotected from O₃ due to the lack of international efforts (Emberson et al.,
598 2014). To be efficient, the mitigation actions for O₃ impacts on biodiversity must be as part of
599 international emission reduction programmes.

600

601 **Acknowledgements**

602 This work was carried out with the contribution of the LIFE financial instrument of the
603 European Union (LIFE15 ENV/IT/183) in the framework of the MOTTLES project
604 “Monitoring ozone injury for setting new critical levels” and published within the
605 International Union of Forest Research Organizations (IUFRO) Task Force on Climate
606 Change and Forest Health.

607

608 **Bibliographic references**

- 609 **Ainsworth E.A.**, Yendrek C.R., Sitch S., Collins, W.J., Emberson L.D., 2012, “The effect of
610 Tropospheric Ozone on Net Primary Productivity and Implications for Climate Change”.
611 *Annu. Rev. Plant Biol.* 63: 637-661
- 612 **Anav A.**, Menut L., Khvorostyanov D., Viovy N., 2011, “Impact of tropospheric ozone on the
613 Euro-Mediterranean vegetation”. *Global Change Biol.* 17: 2342-2359
- 614 **Arbaugh M.J.**, and Bytnerowicz A., 2003, “Ambient ozone patterns and effects over the
615 Sierra Nevada: synthesis and implications for future research”. In: A. Bytnerowicz, M.
616 Arbaugh, R. Alonso (eds), *Ozone Air Pollution in the Sierra Nevada: Distribution and Effects*
617 *on Forests, Developments in Environmental Science*, vol. 2, Elsevier, Amsterdam, 249-261
- 618 **Arneth A.**, Schurgers G., Lathièrè J., Duhl T., Beerling D. J., et al., 2011, “Global terrestrial
619 isoprene emission models: sensitivity to variability in climate and vegetation”. *Atmos. Chem.*
620 *Phys.* 11: 8037-8052
- 621 **Arneth A.**, Schurgers G., Hickler T., Miller P.A., 2008, “Effects of species composition, land
622 surface cover, CO₂ concentration and climate on isoprene emissions from European forests”.
623 *Plant Biol.* 10: 150-162
- 624 **Ashmore M.R.**, 2005, “Assessing the future global impacts of ozone on vegetation”. *Plant*
625 *Cell Environ.* 28: 949-964
- 626 **Ashworth K.**, Wild O., Hewitt C.N., 2013, “Impacts of biofuel cultivation on mortality and
627 crop yields”. *Nat. Clim. Change* 3: 492-496
- 628 **Bassin S.**, Volk M., Fuhrer J., 2013, “Species composition of subalpine grassland is sensitive
629 to nitrogen deposition, but not ozone, after seven years of treatment”. *Ecosystems* 16: 1105-
630 1117
- 631 **Betts R.A.**, Golding N., Gonzalez P., Gornall J., Kahana R., et al., 2015, “Climate and land
632 use change impacts on global terrestrial ecosystems and river flows in the HadGEM2-ES
633 Earth system model using the representative concentration pathways”. *Biogeosciences* 12:
634 1317-1338
- 635 **Bian J.**, Yan R., Chen H., Lü D., Massie S.T., 2011, “Formation of the summertime ozone
636 valley over the Tibetan Plateau: The Asian summer monsoon and air column variations”.
637 *Adv. Atmos. Sci.* 28: 1318-1325
- 638 **Bowman K.W.**, Shindell D.T., Worden H.M., Lamarque J.F., Young P.J., 2013, “Evaluation
639 of ACCMIP outgoing longwave radiation from tropospheric ozone using TES satellite
640 observations”. *Atmos. Chem. Phys.* 13: 4057-4072
- 641 **Clifton O.E.**, Fiore A.M., Correa G., Horowitz L.W., Naik V., 2014, “Twenty-first century
642 reversal of the surface ozone seasonal cycle over the northeastern United States”. *Geophys.*
643 *Res. Lett.* 41: 7343-7350
- 644 **Chen X.L.**, Ma Y.M., Kelder H., Su Z., Yang K., 2011, “On the behaviour of the tropopause
645 folding events over the Tibetan Plateau”. *Atmos. Chem. Phys.* 11: 5113-5122
- 646 **Chevalier A.**, Gheusi F., Delmas R., Ordóñez C., Sarrat C., et al., 2007, “Influence of altitude
647 on ozone levels and variability in the lower troposphere: a ground-based study for Western
648 Europe over the period 2001-2004”. *Atmos. Chem. Phys.* 7: 4311-4326
- 649 **Colette A.**, Granier C., Hodnebrog Ø., Jakobs H., Maurizi A., et al., 2012, “Future air quality
650 in Europe: a multi-model assessment of projected exposure to ozone”. *Atmos. Chem. Phys.*
651 12: 10613-10630
- 652 **Cooper O.R.**, Parrish D.D., Ziemke J., Balashov N.V., Cupeiro M., 2014, “Global
653 distribution and trends of tropospheric ozone: An observation-based review”. *Elementa:*
654 *Science of the Anthropocene* 2: 000029
- 655 **Cooper O.R.**, Sweeney C., Gao R.S., Tarasick D., Leblanc T., 2012, “Long-term ozone
656 trends at rural ozone monitoring sites across the United States, 1990-2010”. *J. Geophys. Res.*
657 117: D22307



- 658 **Cubasch U.**, Wuebbles D., Chen D., Facchini M.C., Frame D., et al., 2013, “Introduction, in
659 Climate Change 2013: The Physical Science Basis”. Contribution of Working Group I to the
660 Fifth Assessment Report of the Intergovernmental Panel on Climate Change, edited by T. F.
661 Stocker et al., Cambridge Univ. Press, Cambridge, U. K. and New York
- 662 **De Marco A.**, Sicard P., Vitale M., Carriero G., Renou C., et al., 2015, “Metrics of ozone risk
663 assessment for Southern European forests: canopy moisture content as a potential plant
664 response indicator”. *Atmos. Environ.* 120: 182-190
- 665 **Derwent R.G.**, Utembe S.R., Jenkin M.E., Shallcross D.E., 2015, “Tropospheric ozone
666 production regions and the intercontinental origins of surface ozone over Europe”. *Atmos.*
667 *Environ.* 112: 216-224
- 668 **Derwent R.G.**, Manning A.J., Simmonds P.G., Spain T.G., O’Doherty S., 2013, “Analysis
669 and interpretation of 25 years of ozone observations at the Mace Head Atmospheric Research
670 Station on the Atlantic Ocean coast of Ireland from 1987 to 2012”. *Atmos. Environ.* 80: 361-
671 368
- 672 **Derwent R.G.**, Witham C.S., Utembe S.R., Jenkin M.E., Passant N.R., 2010, “Ozone in
673 Central England: the impact of 20 years of precursor emission controls in Europe”. *Environ.*
674 *Sci. Policy* 13: 195-204
- 675 **Donner L.J.**, Wyman B.L., Hemler R.S., Horowitz L.W., Ming Y., et al., 2011, “The
676 dynamical core, physical parameterizations, and basic simulation characteristics of the
677 atmospheric component AM3 of the GFDL Global Coupled Model CM3”. *J. Climate* 24:
678 3484-3519
- 679 **European Environment Agency**, 2015 “Air quality in Europe - 2015 report”. ISBN 978-92-
680 9213-702-1. Report No 5/2015
- 681 **Ellingsen K.**, Gauss M., Van Dingenen R., Dentener F.J., Emberson L., et al., 2008, “Global
682 ozone and air quality: a multi-model assessment of risks to human health and crops”. *Atmos.*
683 *Chem. Phys.* 8: 2163-2223
- 684 **Emberson L.D.**, Fuhrer J., Ainsworth L., Ashmore M.R., 2014, “Biodiversity and Ground-
685 level Ozone”. Report UNEP/CBD/SBSTTA/18/INF/17. Convention on Biological Diversity,
686 18th meeting, Montreal, 23-28 June 2014
- 687 **Fares S.**, Vargas R., Detto M., Goldstein A.H., Karlik J., et al., 2013, “Tropospheric ozone
688 reduces carbon assimilation in trees: estimates from analysis of continuous flux
689 measurements”. *Global Change Biol.* 19: 2427-2443
- 690 **Federal Register**, 2015, “National Ambient Air Quality Standards for Ozone”. 40 CFR Part
691 50, 51, 52, 53, and 58, pp 65292-65468
- 692 **Felzer B.S.F.**, Kicklighter D.W., Melillo J.M., Wang C., Zhuang Q., et al., 2004, “Ozone
693 effects on net primary production and carbon sequestration in the conterminous United States
694 using a biogeochemistry model”. *Tellus B* 56: 230-248
- 695 **Fiore A.M.**, Naik V., Leibensperger E.M., 2015, “Air quality and climate connections”. *J. Air*
696 *Waste Manage. Assoc.* 65: 645-685
- 697 **Fiore A.M.**, Naik V., Spracklen D.V., Steiner A., Unger N. et al., 2012, “Global air quality
698 and climate”. *Chem. Soc. Rev.* 41: 6663-6683
- 699 **Fiscus E.L.**, Booker F.L., Burkey K.O., 2005, “Crop responses to ozone: uptake, modes of
700 action, carbon assimilation and partitioning”. *Plant Cell Environ.* 28: 997-1011
- 701 **Gao Y.**, Fu J.S., Drake J.B., Lamarque J.F., Liu Y., 2013, “The impact of emission and
702 climate change on ozone in the United States under representative concentration pathways
703 (RCPs)”. *Atmos. Chem. Phys.* 13: 9607-9621
- 704 **Granier C.**, Niemeier U., Jungclaus J.H., Emmons L., Hess P., et al., 2006, “Ozone pollution
705 from future ship traffic in the Arctic northern passages”. *Geophys. Res. Lett.* 33, doi:
706 10.1029/2006GL026180



- 707 **Guenther A.B.**, Karl T., Harley P., Wiedinmyer C., Palmer P.I., Geron C., 2006, “Estimates
708 of global terrestrial isoprene emissions using MEGAN (Model of Emissions of Gases and
709 Aerosols from Nature)”. *Atmos. Chem. Phys.* 6: 3181-3210
- 710 **Guenther A.B.**, Hewitt C.N., Erickson D., Fall R., Geron, C., et al., 1995, “A global model of
711 natural volatile organic compound emissions”. *J. Geophys. Res.* 100: 8873-8892
- 712 **Guo D.**, Su Y., Shi C., Xunn J., Powell Jr. A.M., 2015, “Double core of ozone valley over the
713 Tibetan Plateau and its possible mechanisms”. *Journal of Atmospheric and Solar-Terrestrial
714 Physics* 130: 127-131
- 715 **Heggin M.I.** and Shepherd T.G., 2009, “Large climate-induced changes in ultraviolet index
716 and stratosphere-to-troposphere ozone flux”. *Nature Geosci.* 2: 687
- 717 **Helmig D.**, Oltmans S.J., Morse T.O., Dibb J.E., 2007, “What is causing high ozone at
718 Summit, Greenland?”. *Atmos. Environ.* 41: 5031-5043
- 719 **Hendriks C.**, Forsell N., Kieseewetter G., Schaap M., Schöpp W., 2016, “Ozone
720 concentrations and damage for realistic future European climate and air quality scenarios”.
721 *Atmos. Environ.* 144: 208-219
- 722 **Hess P.G.** and Zbinden R., 2013, “Stratospheric impact on tropospheric ozone variability and
723 trends: 1990-2009”. *Atmos. Chem. Phys.* 13: 649-674
- 724 **Holland M.**, Kinghorn S., Emberson L., Cinderby S., Ashmore M., et al., 2006,
725 “Development of a framework for probabilistic assessment of the economic losses caused by
726 ozone damage to crops in Europe”. UNECE International Cooperative Programme on
727 Vegetation. Contract Report EPG 1/3/205. CEH Project No: C02309NEW
- 728 **Hsu J.** and Prather M.J., 2009, “Stratospheric variability and tropospheric ozone”. *J.
729 Geophys. Res.* 114: D06102
- 730 **Hu X.M.**, Klein Petra M., Xue M. et al., 2013, “Impact of the vertical mixing induced by low-
731 level jets on boundary layer ozone concentration”. *Atmos. Environ.* 70: 123-130
- 732 **Hudson R.D.**, Andrade M.F., Follette M.B., Frolov A.D., 2006, “The total ozone field
733 separated into meteorological regimes – Part II: Northern Hemisphere mid-latitude total ozone
734 trends”. *Atmos. Chem. Phys.* 6: 5183-5191
- 735 **IPCC**, Intergovernmental Panel on Climate Change, 2014, “Summary for Policymakers”. In:
736 “Climate Change 2014: Impacts, Adaptation and Vulnerability”. Contribution of Working
737 Group II to the Fifth Assessment Report of the Intergovernmental Panel on Climate Change.
738 Cambridge University Press, Cambridge, UK
- 739 **Jeričević A.**, Koračin D., Jiang J., Chow J., Watson J., et al., 2013, “Air Quality Study of
740 High Ozone Levels in South California”. Part of the series NATO Science for Peace and
741 Security Series C: Environmental Security. Air Pollution Modeling and its Application XXII:
742 629-633
- 743 **Johnson C.E.**, Collins W.J., Stevenson D.S., Derwent R.G., 1999, “Relative roles of climate
744 and emissions changes on future tropospheric oxidant concentrations”. *J. Geophys. Res.* 104:
745 18631-18645
- 746 **Josse B.**, Simon P., Peuch V.H., 2004, “Radon global simulations with the multiscale
747 chemistry and transport model MOCAGE”. *Tellus-B* 56: 339-356
- 748 **Kawase H.**, Nagashima T., Sudo K., Nozawa T., 2011, “Future changes in tropospheric
749 ozone under Representative Concentration Pathways (RCPs)”. *Geophys. Res. Lett.* 38:
750 L05801
- 751 **Kelly J.**, Makar P.A., Plummer D.A., 2012, “Projections of mid-century summer air-quality
752 for North America: effects of changes in climate and precursor emissions”. *Atmos. Chem.
753 Phys.* 12: 5367-5390
- 754 **Kirtman B.**, Power S.B., Adedoyin J.A., Boer G.J., Bojariu R., et al., 2013, “Near-term
755 climate change: Projections and predictability, in Climate Change 2013: The Physical Science
756 Basis”. Contribution of Working Group I to the Fifth Assessment Report of the



- 757 Intergovernmental Panel on Climate Change, edited by T.F. Stocker et al., Cambridge Univ.
758 Press, Cambridge, U. K., and New York
- 759 **Klingberg J.**, Engardt M., Karlsson P.E., Langner J., Pleijel H., 2014, “Declining ozone
760 exposure of European vegetation under climate change and reduced precursor emissions”.
761 *Biogeosciences* 11: 5269-5283
- 762 **Krinner G.**, Viovy N., de Noblet-Ducoudré N., Ogé J., Polcher J., et al., 2005, “A dynamic
763 global vegetation model for studies of the coupled atmosphere-biosphere system”. *Global*
764 *Biogeochem. Cy.* 19: GB1015
- 765 **Kulkarni P.S.**, Bortoli D., Domingues A., Silva A.M., 2015, “Surface Ozone Variability and
766 Trend over Urban and Suburban Sites in Portugal”. *Aerosol Air Qual. Res.*: 1-15
- 767 **Kulkarni P.S.**, Bortoli D., Salgado R., Anton M., Costa M.J., et al., 2011, “Tropospheric
768 ozone variability over the Iberian Peninsula”. *Atmos. Environ.* 45: 174-182
- 769 **Kvalevag M.M.** and Myrhe G., 2013, “The effect of carbon-nitrogen coupling on the reduced
770 land carbon sink caused by ozone”. *Geophys. Res. Lett.* 40: 3227-3231
- 771 **Lamarque J.F.**, Shindell D.T., Josse B., Young P.J., Cionni I., et al., 2013, “The
772 Atmospheric Chemistry and Climate Model Intercomparison Project (ACCMIP): overview
773 and description of models, simulations and climate diagnostics”. *Geosci. Model Dev.* 6: 179-
774 206
- 775 **Lamarque J.F.**, Emmons L.K., Hess P.G., Kinnison D.E., Tilmes, S., et al., 2012, “CAM-
776 chem: description and evaluation of interactive atmospheric chemistry in the Community
777 Earth System Model”. *Geosci. Model Dev.* 5: 369-411
- 778 **Lamarque J.F.**, Bond T.C., Eyring V., Granier C., Heil A., et al., 2010, “Historical (1850–
779 2000) gridded anthropogenic and biomass burning emissions of reactive gases and aerosols:
780 methodology and application”. *Atmos. Chem. Phys.* 10: 7017-7039
- 781 **Lamarque J.F.**, Hess P.G., Emmons L.K., Buja L.E., Washington W.M., Granier C., 2005,
782 “Tropospheric ozone evolution between 1890 and 1990”. *J. Geophys. Res.* 110: D08304
- 783 **Langner J.**, Engardt M., Baklanov A., Christensen J.H., Gauss M., et al., 2012, “A multi-
784 model study of impacts of climate change on surface ozone in Europe”. *Atmos. Chem. Phys.*
785 12: 10423-10440
- 786 **Lau N.C.**, Leetmaa A., Nath M.J., 2006, “Attribution of atmospheric variations in the 1997-
787 2003 period to SST anomalies in the Pacific and Indian Ocean basins”. *J. Climate* 19: 3607-
788 3628
- 789 **Lee Y.H.** and Adams P.J., 2011, “A fast and efficient version of the two-moment aerosol
790 sectional (TOMAS) global aerosol microphysics model”. *Aerosol Sci. Tech.* 46: 678-689
- 791 **Lefohn A.S.**, Malley C.S., Simon H., Wells B., Xu X., et al., 2017, “Responses of human
792 health and vegetation exposure metrics to changes in ozone concentration distributions in the
793 European Union, United States, and China”. *Atmos. Environ.* 152: 123-145
- 794 **Lefohn A.S.** and Cooper O.R., 2015, “Introduction to the Special Issue on Observations and
795 Source Attribution of Ozone in Rural Regions of the Western United States”. *Atmos. Environ.*
796 109: 279-281.
- 797 **Lefohn A.S.**, Emery C., Shadwick D., Wernli H., Jung J., Oltmans S.J., 2014, “Estimates of
798 background surface ozone concentrations in the United States based on model-derived source
799 apportionment”. *Atmos. Environ.* 84: 275-288.
- 800 **Lefohn A.S.**, Wernli H., Shadwick D., Oltmans S.J., Shapiro M., 2012, “Quantifying the
801 frequency of stratospheric-tropospheric transport affecting enhanced surface ozone
802 concentrations at high- and low-elevation monitoring sites in the United States”. *Atmos.*
803 *Environ.* 62: 646-656
- 804 **Lefohn A.S.**, Shadwick D., Oltmans S.J., 2010, “Characterizing changes in surface ozone
805 levels in metropolitan and rural areas in the United States for 1980-2008 and 1994-2008”.
806 *Atmos. Environ.* 44: 5199-5210



- 807 **Legrand M.**, Preunkert S., Jourdain B., Gallée H., Goutail F., et al., 2009, “Year-round record
808 of surface ozone at coastal (Dumont d’Urville) and inland (Concordia) sites in East
809 Antarctica”. *J. Geophys. Res.* 114: doi: 10.1029/2008JD011667
- 810 **Liu C.**, Liu Y., Cai Z., Gao S., Bian J., et al., 2010, “Dynamic formation of extreme ozone
811 minimum events over the Tibetan Plateau during northern winters 1987-2001”. *J. Geophys.*
812 *Res.* 115: D18311
- 813 **Meinshausen M.**, Wigley T.M.L., Raper S.C.B., 2011, “Emulating atmosphere-ocean and
814 carbon cycle models with a simpler model, MAGICC6 - Part 2: Applications”. *Atmos. Chem.*
815 *Phys.* 11: 1457-1471
- 816 **Mills G.**, Hayes F., Simpson D., Emberson L., Norris D., et al., 2011, “Evidence of
817 widespread effects of ozone on crops and (semi-)natural vegetation in Europe (1990-2006) in
818 relation to AOT40 and flux-based risk maps”. *Global Change Biol.* 17: 592-613
- 819 **Monks P.S.**, Archibald A.T., Colette A., Cooper O., Coyle M., et al., 2015, “Tropospheric
820 ozone and its precursors from the urban to the global scale from air quality to short-lived
821 climate forcer”. *Atmos. Chem. Phys.* 15: 8889-8973
- 822 **Myhre G.**, Shindell D., Bréon F.M., Collins W., Fuglestedt J., et al., 2013, “Anthropogenic
823 and Natural Radiative Forcing”. In: *Climate Change 2013: The Physical Science Basis.*
824 *Contribution of Working Group I to the Fifth Assessment Report of the Intergovernmental*
825 *Panel on Climate Change.* Cambridge University Press, Cambridge, United Kingdom and
826 New York, USA
- 827 **Naik V.**, Voulgarakis A., Fiore A.M., Horowitz L.W., Lamarque J.F., et al., 2012,
828 “Preindustrial to present day changes in tropospheric hydroxyl radical and methane lifetime
829 from the Atmospheric Chemistry and Climate Model Intercomparison Project (ACCMIP)”.
830 *Atmos. Chem. Phys. Discuss.* 12: 30755-30804
- 831 **Nazarenko L.**, Schmidt G.A., Miller R.L., Tausnev N., Kelley M., et al., 2015, “Future
832 climate change under RCP emission scenarios with GISS ModelE2”. *J. Adv. Model. Earth*
833 *Syst.* 7: 244-267
- 834 **Nemani R.R.**, Keeling C.D., Hashimoto H., Jolly W.M., Piper S.C., et al., 2003, “Climate-
835 Driven Increases in Global Terrestrial Net Primary Production from 1982 to 1999”. *Science*
836 300: 1560-1563
- 837 **Ollinger S.V.**, Aber J.D., Reich P.B., 1997, “Simulating ozone effects on forest productivity:
838 interactions among leaf, canopy, and stand-level processes”. *Ecol. Appl.* 7: 1237-1251.
- 839 **Oltmans S.J.**, Lefohn A.S., Harris J.M., Galbally I., Scheel H.E., et al., 2006, “Long-term
840 changes in tropospheric ozone”. *Atmos. Environ.* 40: 3156-3173
- 841 **Paoletti E.**, De Marco A., Beddows D.C.S., Harrison R.M., Manning W.J., 2014, “Ozone
842 levels in European and USA cities are increasing more than at rural sites, while peak values
843 are decreasing”. *Environ. Pollut.* 192: 295-299
- 844 **Paoletti E.**, Contran N., Bernasconi P., Günthardt-Goerg M.S., Vollenweider P., 2009,
845 “Structural and physiological responses to ozone in Manna ash (*Fraxinus ornus L.*) leaves in
846 seedlings and mature trees under controlled and ambient conditions”. *Sci. Total Environ.* 407:
847 1631-1643
- 848 **Paoletti E.** and Manning W.J., 2007, “Toward a biologically significant and usable standard
849 for ozone that will also protect plants”. *Environ. Pollut.* 150: 85-95
- 850 **Paoletti E.**, 2006, “Impact of ozone on Mediterranean forest: A review”. *Environ. Pollut.* 144:
851 463-474
- 852 **Parrish D.D.**, Law K.S., Staehelin J., Derwent R., Cooper O.R., et al., 2012, “Long-term
853 changes in lower tropospheric baseline ozone concentrations at northern mid-latitudes”.
854 *Atmos. Chem. Phys.* 12: 11485-11504
- 855 **Pfister G.G.**, Walters S., Lamarque J.F., Fast J., Barth M.C., et al., 2014, “Projections of
856 future summertime ozone over the U.S”. *J. Geophys. Res. Atmos.* 119: 5559-5582



- 857 **Price C.** and Rind D.H., 1992, “A simple lightning parameterization for calculating global
858 lightning distributions”. *J. Geophys. Res.*, 97: 9919-9933
- 859 **Proietti C.**, Anav A., De Marco A., Sicard P., Vitale M., 2016, “A multi-sites analysis on the
860 ozone effects on Gross Primary Production of European forests”. *Sci. Total Environ.* 556: 1-
861 11
- 862 **Querol X.**, Alastuey A., Pandolfi M., Reche C., Pérez N., et al., 2014, “2001-2012 trends on
863 air quality in Spain”. *Sci. Total Environ.* 490: 957-969.
- 864 **Reich P.B.**, 1987, “Quantifying plant response to ozone: a unifying theory”. *Tree Physiol.* 3:
865 63-91
- 866 **Ren W.**, Tian H., Liu M., Zhang C., Chen G., et al., 2007, “Effects of tropospheric ozone
867 pollution on net primary productivity and carbon storage in terrestrial ecosystems of China”.
868 *J. Geophys. Res.* 112: 1-17
- 869 **Revell L.E.**, Tummon F., Stenke A., Sukhodolov T., Coulon A., et al., 2015, “Drivers of the
870 tropospheric ozone budget throughout the 21st century under the medium-high climate
871 scenario RCP 6.0”. *Atmos. Chem. Phys.* 15: 5887-5902
- 872 **Riahi K.**, Rao S., Krey V., Cho C., Chirkov V., et al., 2011, “RCP 8.5 - A scenario of
873 comparatively high greenhouse gas emissions”. *Climatic Change* 109: 33-57
- 874 **Rieder H.E.**, Fiore A.M., Horowitz L.W., Naik V., 2015, “Projecting policy-relevant metrics
875 for high summertime ozone pollution events over the eastern United States due to climate and
876 emission changes during the 21st century”. *J. Geophys. Res. Atmos.* 120: 784-800
- 877 **Ridley B.A.**, Pickering K.E., Dye, J.E., 2005, “Comments on the parameterization of
878 lightning-produced NO in global chemistry-transport models”. *Atmos. Environ.* 39: 6184-
879 6187
- 880 **Sanderson M.G.**, Collins W.J., Hemming D.L., Betts R.A., 2007, “Stomatal conductance
881 changes due to increasing carbon dioxide levels: Projected impact on surface ozone levels”.
882 *Tellus* 59B: 404-411
- 883 **Sanderson M.G.**, Jones C.D., Collins W.J., Johnson C.E., Derwent R.G., 2003, “Effect of
884 climate change on isoprene emissions and surface ozone levels”. *Geophys. Res. Lett.* 30: 1936
- 885 **Schnell J.L.**, Prather M.J., Josse B., Naik V., Horowitz L.W., et al., 2016, “Effect of climate
886 change on surface ozone over North America, Europe, and East Asia”. *Geophys. Res. Lett.* 43:
887 L068060
- 888 **Seidel D.J.**, Fu Q., Randel W.J., Reichler T.J., 2008, “Widening of the tropical belt in a
889 changing climate”. *Nat. Geosci* 1: 21-4
- 890 **Shindell D.T.**, Lamarque J.F., Schulz M., Flanner M., Jiao C., et al., 2012, “Radiative forcing
891 in the ACCMIP historical and future climate simulations”. *Atmos. Chem. Phys. Discuss.* 12:
892 21105-21210
- 893 **Shindell D.T.**, Faluvegi G., Stevenson D.S., Krol M.C., Emmons L.K., et al., 2006, “Multi-
894 model simulations of carbon monoxide: Comparison with observations and projected near-
895 future changes”. *J. Geophys. Res.* 111: D19306
- 896 **Sicard P.**, Serra R., Rossello P., 2016a, “Spatiotemporal trends of surface ozone
897 concentrations and metrics in France”. *Environ. Res.* 149: 122-144
- 898 **Sicard P.**, Augustaitis A., Belyazid S., Calfapietra C., De Marco A., et al., 2016b, “Global
899 topics and novel approaches in the study of air pollution, climate change and forest
900 ecosystems”. *Environ. Pollut.* 213: 977-987
- 901 **Sicard P.**, De Marco A., Dalstein-Richier L., Tagliaferro F., Paoletti E., 2016c, “An
902 epidemiological assessment of stomatal ozone flux-based critical levels for visible ozone
903 injury in Southern European forests”. *Sci. Total Environ.* 541: 729-741
- 904 **Sicard P.**, De Marco A., Troussier F., Renou C., Vas N., Paoletti E., 2013, “Decrease in
905 surface ozone concentrations at Mediterranean remote sites and increase in the cities”. *Atmos.*
906 *Environ.* 79: 705-715



- 907 **Sicard P.**, Vas N., Dalstein-Richier L., 2011, “Annual and seasonal trends for ambient ozone
908 concentration and its Impact on Forest Vegetation in Mercantour National Park (South-eastern
909 France) over the 2000-2008 period”. *Environ. Pollut.* 159: 351-362
- 910 **Sicard P.**, Coddeville P., Galloo J.C., 2009, “Near-surface ozone levels and trends at rural
911 stations in France over the 1995-2003 period”. *Environ. Monit. Assess.* 156: 141-157
- 912 **Simpson D.**, Arneft A., Mills G., Solberg S., Uddling J., 2014, “Ozone - the persistent
913 menace: interactions with the N cycle and climate change”. *Curr. Opin. Env. Sust.* 9-10: 9-19
- 914 **Singh H.B.**, Herlth D., O'Hara D., Zahnle K., Bradshaw J.D., et al., 1992, “Relationship of
915 Peroxyacetyl nitrate to active and total odd nitrogen at northern high latitudes: influence of
916 reservoir species on NO_x and O₃”. *J. Geophys. Res.* 97:16523-30
- 917 **Sitch S.**, Cox P.M., Collins W.J., Huntingford C., 2007, “Indirect radiative forcing of climate
918 change through ozone effects on the land-carbon sink”. *Nature* 448: 791-794
- 919 **Steinbacher M.**, Henne S., Dommen J., Wiesen P., Prevot A.S.H., 2004, “Nocturnal trans-
920 alpine transport of ozone and its effects on air quality on the Swiss Plateau”. *Atmos. Environ.*
921 38: 4539-4550
- 922 **Stevenson D.S.**, Young P.J., Naik V., Lamarque J.F., Shindell D.T., et al., 2013,
923 “Tropospheric ozone changes, radiative forcing and attribution to emissions in the
924 Atmospheric Chemistry and Climate Model Inter-comparison Project (ACCMIP)”. *Atmos.*
925 *Chem. Phys.* 13: 3063-3085
- 926 **Stevenson D.S.**, Young P.J., Naik V., Lamarque J.F., Shindell D.T., et al., 2012,
927 “Tropospheric ozone changes, radiative forcing and attribution to emissions in the
928 Atmospheric Chemistry and Climate Model Inter-comparison Project (ACCMIP)”. *Atmos.*
929 *Chem. Phys. Discuss.* 12: 26047-26097
- 930 **Stevenson D.S.**, Dentener F.J., Schultz M.G., Ellingsen K., van Noije T.P.C., et al., 2006,
931 “Multi-model ensemble simulations of present-day and near-future tropospheric ozone”. *J.*
932 *Geophys. Res.* 111: D08301
- 933 **Stevenson D.S.**, Johnson C.E., Collins W.J., Derwent R.G., Edwards J.M., 2000, “Future
934 estimates of tropospheric ozone radiative forcing and methane turnover – The impact of
935 climate change”. *Geophys. Res. Lett.* 27: 2073-2076
- 936 **Stohl A.**, Berg T., Burkhart J.F., Fjaeraa A.M., Forster C., et al., 2007, « Arctic smoke -
937 record high air pollution levels in the European Arctic due to agricultural fires in Eastern
938 Europe in spring 2006”. *Atmos. Chem. Phys.* 7: 511-534
- 939 **Tang Q.**, Prather M.J., Hsu J., 2011, “Stratosphere-troposphere exchange ozone flux related
940 to deep convection”. *Geophys. Res. Lett.* 38: L03806
- 941 **Teyssède H.**, Michou M., Clark H.L., Josse B., Karcher F., et al., 2007, “A new tropospheric
942 and stratospheric Chemistry and Transport Model MOCAGE-Climat for multi-year studies:
943 evaluation of the present-day climatology and sensitivity to surface processes”. *Atmos. Chem.*
944 *Phys.* 7: 5815-5860
- 945 **Tian W.**, Chipperfield M., Huang Q., 2008, “Effects of the Tibetan Plateau on total column
946 ozone distribution”. *Tellus* 60B: 622-635
- 947 **UNECE**, United Nations Economic Commission for Europe. Convention on Long-Range
948 Trans-boundary Air Pollution, 2010, “Mapping Critical Levels for Vegetation”. International
949 Cooperative Programme on Effects of Air Pollution on Natural Vegetation and Crops,
950 Bangor, UK
- 951 **van Vuuren D.**, Edmonds J., Kainuma M., Riahi K., Thomson A., et al., 2011, “The
952 representative concentration pathways: an overview”. *Climatic Change* 109: 5-31
- 953 **Voulgarakis A.**, Naik V., Lamarque J.F., Shindell D.T., Young P.J. et al., 2013, “Analysis of
954 present day and future OH and methane lifetime in the ACCMIP simulations”. *Atmos. Chem.*
955 *Phys.* 13: 2563-2587



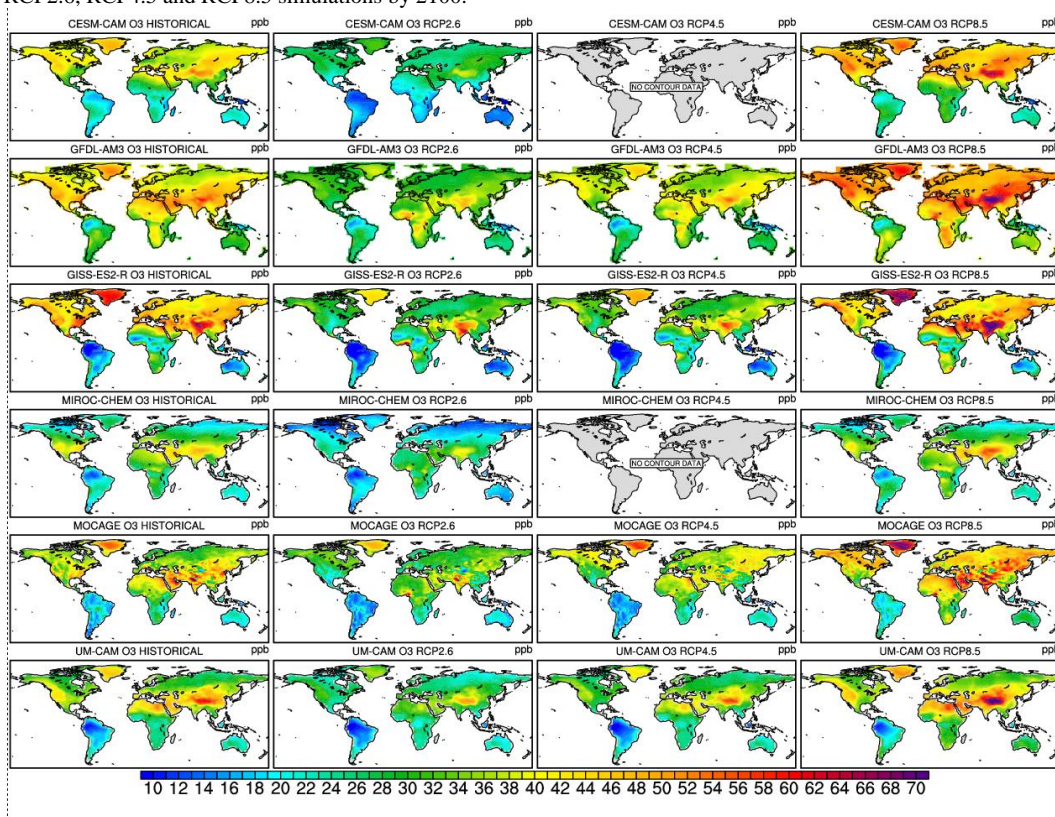
- 956 **Walker T.W.**, Jones D.B.A., Parrington M., Henze D.K., Murray L.T., et al., 2012, “Impacts
957 of mid-latitude precursor emissions and local photochemistry on ozone abundances in the
958 Arctic”. *Journal of Geophysical Research: Atmospheres* 117, doi: 10.1029/2011JD016370
- 959 **Wang Q.Y.**, Gao R.S., Cao J.J., Schwarz J.P., Fahey D.W., et al. 2015, “Observations of high
960 level of ozone at Qinghai Lake basin in the northeastern Qinghai-Tibetan Plateau, western
961 China”. *J. Atm. Chem.* 72: 19-26
- 962 **Wang X.** and Mauzerall D.L., 2004, “Characterizing distributions of surface ozone and its
963 impact on grain production in China, Japan and South Korea: 1900 and 2020”. *Atmos.*
964 *Environ.* 38: 4383-4402
- 965 **Watanabe S.**, Hajima T., Sudo K., Nagashima T., Takemura T., et al., 2011, “MIROC-ESM
966 2010: model description and basic results of CMIP5-20c3m experiments”. *Geosci. Model*
967 *Dev.* 4: 845-872
- 968 **Wesely M.L.** and Hicks B.B., 2000, “A review of the current status of knowledge in dry
969 deposition”. *Atmos. Environ.* 34: 2261-2282
- 970 **Wild O.**, Fiore A.M., Shindell D.T., Doherty R.M., Collins W.J., et al., 2012, “Modelling
971 future changes in surface ozone: a parameterized approach”. *Atmos. Chem. Phys.* 12: 2037-
972 2054
- 973 **Wild O.**, 2007, “Modelling the global tropospheric ozone budget: exploring the variability in
974 current models”. *Atmos. Chem. Phys.* 7: 2643-2660
- 975 **Williams E.R.**, 2009, “The global electrical circuit: A review”. *Atmos. Res.*, 91: 140-152.
- 976 **Wilson R.C.**, Fleming Z. L., Monks P. S., Clain G., Henne S., et al., 2012, “Have primary
977 emission reduction measures reduced ozone across Europe? An analysis of European rural
978 background ozone trends 1996-2005”. *Atmos. Chem. Phys.* 12: 437-454
- 979 **Wittig V.E.**, Ainsworth E.A., Naidu S.L., Karnosky D.F., Long S.P., 2009, “Quantifying the
980 impact of current and future tropospheric ozone on tree biomass, growth, physiology and
981 biochemistry: a quantitative meta-analysis”. *Global Change Biol.* 15: 396-424
- 982 **Wittig V.E.**, Ainsworth E.A., Long S.P., 2007, “To what extent do current and projected
983 increases in surface ozone affect photosynthesis and stomatal conductance of trees? A meta-
984 analytic review of the last 3 decades of experiments”. *Plant, Cell Environ.* 30: 1150-1162
- 985 **Xing J.**, Mathur R., Pleim J., C. Hogrefe, Gan C.M., et al., 2015, “Observations and modeling
986 of air quality trends over 1990–2010 across the Northern Hemisphere: China, the United
987 States and Europe”. *Atmos. Chem. Phys.* 15: 2723-2747
- 988 **Young P.J.**, Archibald A.T., Bowman K.W., Lamarque J.F., Naik V., et al., 2013,
989 “Preindustrial to end 21st century projections of tropospheric ozone from the Atmospheric
990 Chemistry and Climate Model Intercomparison Project (ACCMIP)”. *Atmos. Chem. Phys.* 13:
991 2063-2090
- 992 **Zak D.R.**, Pregitzer K.S., Kubiske M.E., Burton A.J., 2011, “Forest productivity under
993 elevated CO₂ and O₃: positive feedbacks to soil N cycling sustain decade-long net primary
994 productivity enhancement by CO₂. *Ecology Letters* 14: 1220-1226
- 995 **Zeng G.**, Morgenstern O., Braesicke P., Pyle J.A., 2010, “Impact of stratospheric ozone
996 recovery on tropospheric ozone and its budget”. *Geophys. Res. Lett.* 37: L09805
- 997 **Zeng G.**, Pyle J.A., Young P. J., 2008, “Impact of climate change on tropospheric ozone and
998 its global budgets, *Atmos. Chem. Phys.* 8: 369-387
- 999 **Zeng G.** and Pyle J.A., 2003, “Changes in tropospheric ozone between 2000 and 2100
1000 modeled in a chemistry-climate model”. *Geophys. Res. Lett.* 30: 1392
- 1001 **Zhang Q.**, Streets D.G., Carmichael G.R., He K.B., Huo H., et al., 2009, “Asian emissions in
1002 2006 for the NASA INTEX-B mission”. *Atmos. Chem. Phys.* 9: 5131-5153
- 1003 **Zhang M.**, Xu Y., Uno I., Akimoto H., 2004, “A numerical study of tropospheric ozone in the
1004 springtime in east Asia”. *Adv. Atmos. Sci.* 21: 163-170



- 1005 **Zhang L.**, Brook J. R., Vet R., 2003, “A revised parameterization for gaseous dry deposition
1006 in air-quality models”. Atmos. Chem. Phys. 3: 2067-2082
1007 **Zhu Z.**, Piao S., Myneni R.B., Huang M., Zeng Z., et al., 2016, “Greening of the Earth and its
1008 drivers”. Nature Climate Change 6: 791-795



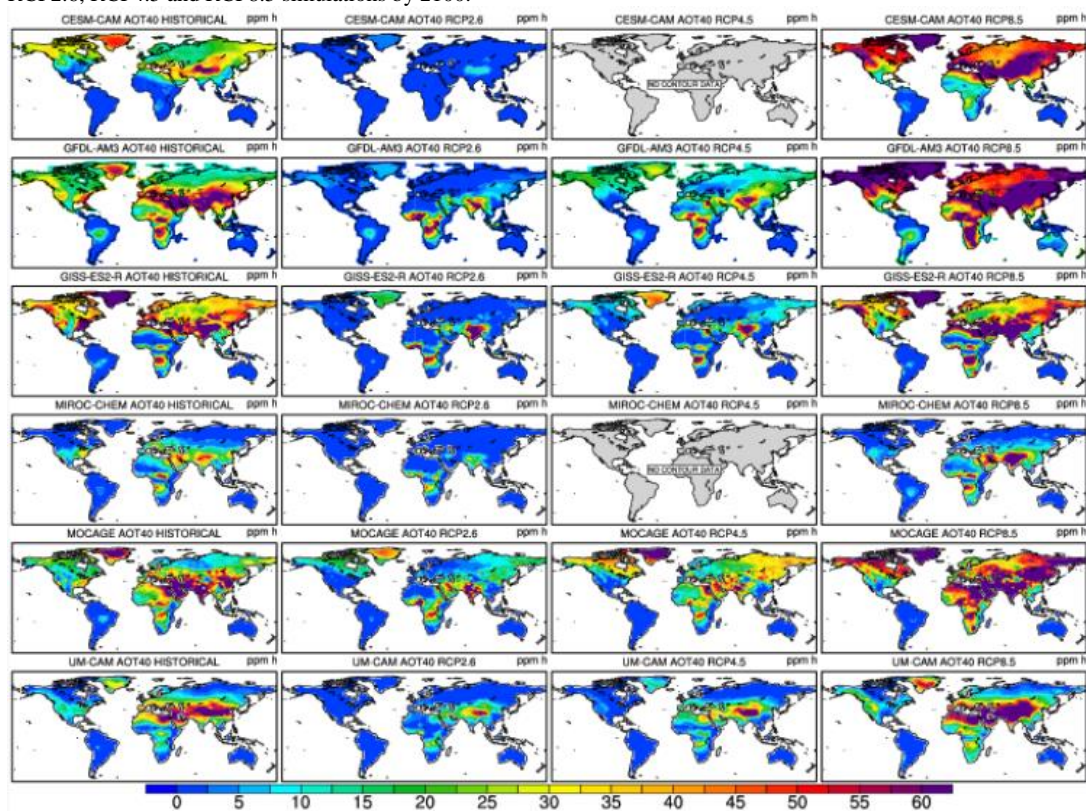
1009 **Figure 1:** Surface ozone mean concentrations (in ppb) at the lower model layer for each ACCMIP model for the historical run and
1010 for RCP2.6, RCP4.5 and RCP8.5 simulations by 2100.



1011



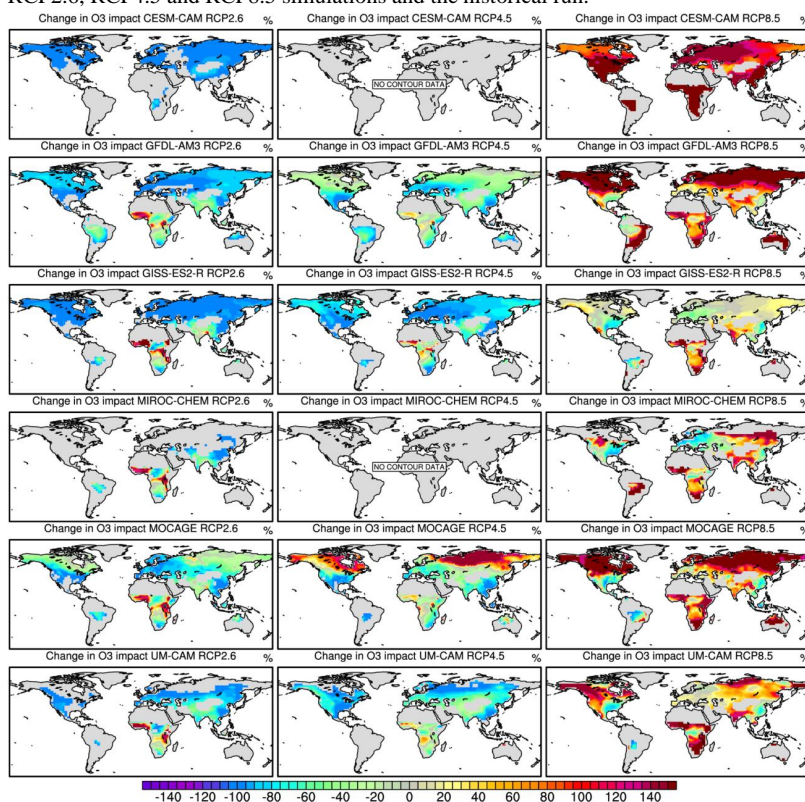
1012 **Figure 2:** Surface AOT40 means (in ppm.h) at the lower model layer for each ACCMIP model for the historical run and for
1013 RCP2.6, RCP4.5 and RCP8.5 simulations by 2100.



1014



1015 **Figure 3:** Simulated percentage changes (%) in the potential ozone impact on vegetation (IO3) for each ACCMIP model between
1016 RCP2.6, RCP4.5 and RCP8.5 simulations and the historical run.



1017



1018 **Table 1:** Characteristics of the models, including simulation time slice, spatial resolution, simulated gas species and associated
 1019 bibliographic references (from Lamarque et al., 2013 and Young et al. 2013). Black carbon (BC), Organic carbon (OC), Secondary
 1020 Organic Aerosols (SOA), Dimethylsulfide (DMS), Chemistry Climate Model (CCM), Chemistry Transport Model (CTM),
 1021 Chemistry-General Circulation Model (CGCM).
 1022

Models	Type	Simulation length	Resolution (lat/lon)	Number of vertical pressure levels & top level	Species simulated	References
CESM-CAM	CCM	2000-2009 and 2100-2109	1.875/2.5	26 levels 3.5 hPa	16 gas species; constant present-day isoprene, soil NO _x , DMS and volcanic sulfur, oceanic CO.	Lamarque et al., 2012
GFDL-AM3	CCM	2001-2010 and 2101-2110	2.0/2.5	48 levels 0.017 hPa	81 gas species; SO _x , BC, OC, SOA, NH ₃ , NO ₃ ; constant pre-industrial soil NO _x ; constant present-day soil and oceanic CO, and biogenic VOC; climate-sensitive dust, sea salt, and DMS.	Donner et al., 2011 Naik et al., 2012
GISS-E2-R	CCM	2000-2004 and 2101-2105	2.0/2.5	40 levels 0.14 hPa	51 gas species; interactive sulfate, BC, OC, sea salt, dust, NO ₃ , SOA, alkenes; constant present-day soil NO _x ; climate-sensitive dust, sea salt, and DMS; climate-sensitive isoprene based on present-day vegetation.	Lee and Adams, 2011 Shindell et al., 2012
MIROC-CHEM	CCM	2000-2010 and 2100-2104	2.8/2.8	80 levels 0.003 hPa	58 gas species; SO ₄ , BC, OC; constant present-day VOCs, soil-NO _x , oceanic-CO; climate-sensitive dust, sea salt and DMS.	Watanabe et al., 2011
MOCAGE	CTM	2000-2003 and 2100-2103	2.0/2.0	47 levels 6.9 hPa	110 gas species; constant present-day isoprene, other VOCs, oceanic CO and soil NO _x .	Josse et al., 2004 Krinner et al., 2005 Teyssèdre et al., 2007
UM-CAM	CGCM	2000-2005 and 2094-2099	2.50/3.75	19 levels 4.6 hPa	60 gas species; constant present-day biogenic isoprene, soil NO _x , biogenic and oceanic CO.	Zeng et al., 2008, 2010

1023



1024 **Table 2a:** Annual total emissions of CO (Tg CO/year), NMVOCs (Tg C/year), NO_x (Tg N/year, including lightning and soil NO_x),
 1025 total lightning NO_x emissions (LNO_x) and global atmospheric methane (CH₄) burden (Tg) for the historical simulations in each
 1026 model (from Young et al., 2013 and * from Voulgarakis et al., 2013).

1027
 1028
 1029
 1030
 1031
 1032
 1033
 1034
 1035
 1036
 1037

Models	Historical				
	CO	*CH ₄	NMVOCs	NO _x	*LNO _x
CESM-CAM	1248	4902	429	50.0	4.2
GFDL-AM3	1246	4809	830	46.2	4.4
GISS-E2-R	1070	4793	830	48.6	7.7
MIROC-CHEM	1064	4805	833	57.3	9.7
MOCAGE	1168	4678	1059	47.9	5.2
UM-CAM	1148	4879	535	49.2	5.1

1038 **Table 2b:** Simulated percentage (%) changes in total emissions of CO, NMVOCs, NO_x (including lightning and soil NO_x), total
 1039 lightning NO_x emissions (LNO_x) and global atmospheric CH₄ burden for each model between 2100 and historical simulation for
 1040 RCPs (from Young et al., 2013 and *Voulgarakis et al., 2013). The last row shows means and standard deviations (SD). Missing or
 1041 not available data are identified (n.a).
 1042

Models	RCP2.6 scenario					RCP4.5 scenario					RCP8.5 scenario				
	CO	*CH ₄	VOCs	NO _x	*LNO _x	CO	*CH ₄	VOCs	NO _x	*LNO _x	CO	*CH ₄	VOCs	NO _x	*LNO _x
CESM-CAM	-36.7	-27.1	0	-52.8	+7.1	n.a	n.a	n.a	n.a	n.a	-30.1	+112.1	0	-33.0	+29.7
GFDL-AM3	-36.9	-27.9	-5.0	-47.0	+12.6	-47.4	-9.3	-3.6	-41.5	+23.5	-30.3	+116.1	-1.9	-22.4	+38.2
GISS-E2-R	-42.8	-21.0	+0.5	-44.2	+3.8	-54.9	+4.6	+6.9	-39.2	+12.2	-35.1	+152.7	+19.8	-20.0	+26.2
MIROC-CHEM	-43.1	-28.2	-7.1	-36.0	+7.5	n.a	n.a	n.a	n.a	n.a	-35.4	+116.0	-3.4	-6.9	+38.0
MOCAGE	-39.4	-28.8	-6.5	-45.7	+5.2	n.a	n.a	n.a	n.a	n.a	-32.3	+113.4	-2.8	-22.9	+19.9
UM-CAM	-39.0	-27.9	-11.3	-40.6	+8.1	-50.4	-8.7	-9.2	-36.0	+17.5	-32.0	+112.1	-4.2	-17.2	+43.6
Mean ± SD	-39.7 ± 2.2	-26.8 ± 3.7	-4.9 ± 4.9	-44.4 ± 4.3	+7.4 ± 2.0	-50.9 ± 3.2	-4.5 ± 9.4	-2.0 ± 11.4	-38.9 ± 2.3	+17.7 ± 3.7	-32.5 ± 1.8	+120.4 ± 19.5	+1.3 ± 11.6	-20.4 ± 7.0	+32.6 ± 10.8

1043
 1044



1045 **Table 3a:** Global and hemispheric (averaged over the domain) surface ozone mean concentrations (in ppb) and AOT40 means (in
 1046 ppm.h) for the historical simulations in each model (North and South Hemisphere, i.e NH and SH). The last row shows means and
 1047 standard deviations (SD).
 1048

Models	Ozone conc. global	Ozone conc. SH	Ozone conc. NH	AOT40 global	AOT40 SH	AOT40 NH
CESM-CAM	31.3	20.9	36.4	12.8	0.2	18.9
GFDL-AM3	38.6	30.6	42.9	21.8	4.7	30.8
GISS-E2-R	35.8	22.3	42.3	26.0	3.6	36.8
MIROC-CHEM	27.9	20.4	31.4	7.3	1.9	9.8
MOCAGE	32.9	21.5	38.3	22.9	3.5	31.8
UM-CAM	31.3	21.4	36.0	14.4	1.3	20.6
Mean ± SD	33.0 ± 3.8	22.9 ± 3.8	37.9 ± 4.3	17.5 ± 7.2	2.5 ± 1.7	24.8 ± 10.1

1049
 1050
 1051
 1052
 1053
 1054
 1055
 1056

Table 3b: Simulated percentage (%) changes in global and hemispheric surface ozone mean concentrations and in global mean
 stratospheric ozone column (* from Voulgarakis et al., 2013) for each model between 2100 and historical simulation for RCPs
 (North and South Hemisphere, i.e NH and SH). The last row shows means and standard deviations (SD). Missing or not available
 data are identified (n.a).

Models	Surface ozone mean concentrations									* Stratospheric ozone		
	RCP2.6 global	RCP2.6 SH	RCP2.6 NH	RCP4.5 global	RCP4.5 SH	RCP4.5 NH	RCP8.5 global	RCP8.5 SH	RCP8.5 NH	RCP2.6 global	RCP4.5 global	RCP8.5 global
CESM-CAM	-29.1	-20.6	-31.3	n.a	n.a	n.a	+21.9	+22.5	+20.5	n.a	n.a	+5.3
GFDL-AM3	-20.5	-10.8	-24.5	-11.7	-6.9	-13.5	+15.5	+18.6	+14.5	+3.3	+3.9	+8.4
GISS-E2-R	-23.5	-5.8	-27.9	-20.4	-6.3	-23.9	+7.0	+19.3	+3.8	+8.0	+8.8	+15.1
MIROC-CHEM	-23.3	-12.3	-26.8	n.a	n.a	n.a	+3.9	+10.3	+2.2	+2.6	n.a	+4.2
MOCAGE	-12.8	+7.4	-18.5	-1.8	+17.7	-7.0	+23.1	+40.4	+16.7	+19.9	n.a	+23.6
UM-CAM	-17.3	-4.7	-21.1	-8.3	+0.9	-10.8	+14.4	+24.3	+11.4	+6.7	+6.9	+7.4
Mean± SD	-21.1 ± 5.6	-7.8 ± 9.4	-25.0 ± 4.7	-10.5 ± 7.7	+1.4 ± 11.5	-13.8 ± 7.2	+13.8 ± 7.1	+22.6 ± 10.0	+11.5 ± 7.3	+8.1 ± 7.0	+6.5 ± 2.5	+10.7 ± 7.4

1057
 1058



1059 **Table 3c:** Simulated percentage (%) changes in global and hemispheric AOT40 means for each model between 2100 and historical
 1060 simulation for RCPs (North and South Hemisphere, i.e NH and SH). Missing or not available data are identified (n.a).
 1061

Models	AOT40								
	RCP2.6 global	RCP2.6 SH	RCP2.6 NH	RCP4.5 global	RCP4.5 SH	RCP4.5 NH	RCP8.5 global	RCP8.5 SH	RCP8.5 NH
CESM-CAM	-96.9	-99.9	-96.8	n.a	n.a	n.a	+138.3	+150.0	+134.9
GFDL-AM3	-75.2	-25.5	-78.9	-53.2	-36.2	-54.5	+96.3	+242.5	+85.1
GISS-E2-R	-78.1	-13.9	-81.2	-75.0	-27.8	-77.2	+22.3	+83.3	+19.5
MIROC-CHEM	-74.0	-10.5	-80.6	n.a	n.a	n.a	+20.5	+78.9	+16.3
MOCAGE	-53.7	+68.6	-59.7	-17.5	+202.9	-28.3	+85.1	+448.6	+67.0
UM-CAM	-73.6	+92.3	-76.7	-52.8	+7.7	-54.8	+49.3	+176.9	+45.1
Mean ± SD	-75.2 ± 13.7	+1.9 ± 69.5	-79.0 ± 11.8	-49.6 ± 23.8	+36.6 ± 112.4	-53.7 ± 20.0	+68.6 ± 46.3	+196.7 ± 137.7	+61.3 ± 44.8

1062

1063

1064 **Table 3d:** Simulated percentage (%) changes in potential O₃ impact on vegetation (IO3) for each model between 2100 and historical
 1065 simulation for RCPs (North and South Hemisphere, i.e NH and SH). Missing or not available data are identified (n.a).
 1066

Models	Risk factor IO3								
	RCP2.6 global	RCP2.6 SH	RCP2.6 NH	RCP4.5 global	RCP4.5 SH	RCP4.5 NH	RCP8.5 global	RCP8.5 SH	RCP8.5 NH
CESM-CAM	-97.2	-91.8	-97.5	n.a	n.a	n.a	+129.6	+146.8	+127.5
GFDL-AM3	-69.4	-49.1	-74.8	-50.1	-61.1	-47.2	+91.9	+95.5	+90.4
GISS-E2-R	-66.1	-20.7	-74.3	-71.7	-53.3	-74.6	+21.5	+56.6	+14.2
MIROC-CHEM	-41.4	-18.9	-51.9	n.a	n.a	n.a	+41.0	+103.8	+25.5
MOCAGE	-46.6	-22.8	-51.4	-7.0	-38.0	-1.0	+77.7	+68.2	+80.0
UM-CAM	-45.8	-9.2	-71.3	-59.5	+2.0	-69.0	+61.3	+84.2	+56.0
Mean ± SD	-61.1 ± 21.1	-35.5 ± 30.7	-70.2 ± 17.2	-47.1 ± 28.1	-37.6 ± 28.1	-47.9 ± 33.4	+70.5 ± 38.4	+92.5 ± 31.7	+65.6 ± 42.4

1067